[American Journal of Science, Vol. 317, October, 2017, P. 941–964, DOI 10.2475/08.2017.03]

ARC MAGMATISM WITNESSED BY DETRITAL ZIRCON U-Pb GEOCHRONOLOGY, Hf ISOTOPES AND PROVENANCE ANALYSIS OF LATE CRETACEOUS-MIOCENE SANDSTONES OF ONSHORE WESTERN MAKRAN (SE IRAN)

ALI MOHAMMADI[*,†], JEAN-PIERRE BURG[*], MARCEL GUILLONG[*], and ALBRECHT VON QUADT[*]

ABSTRACT. The present work aims to contribute to the Cenozoic tectonic setting of the western part of the Makran Accretionary Wedge in SE Iran. We determine the provenance of both deep marine turbiditic and deltaic-shelf Late Cretaceous-Miocene sandstones, describe the sandstone modal framework and heavy minerals and report a new geochronological and isotopic study including 2307 detrital zircons U-Pb ages and 204 *in-situ* Hf isotopic analyses. Modal sandstone framework compositions indicate that a magmatic arc and recycled accreted sediments were the main sources of Eocene-Oligocene and Miocene sandstones. Cr-spinel and heavy mineral assemblages indicate ultramafic rocks, likely ophiolitic mantle, as a subsidiary source. Detrital zircon U-Pb ages cluster in five main age groups: (1) Neoproterozoic grains suggesting a continental crust provenance within the Central Iran blocks, (2) Jurassic grains with Hf isotopic compositions of continental crust, suggesting a rifting related magmatic provenance, (3) Late Cretaceous and (4) Eocene grains, with Hf isotopic compositions typical of continental crust and non-depleted mantle, suggesting a continental magmatic arc provenance, and (5) Early Miocene grains. The new U-Pb age and Hf isotopic ratios correspond to those obtained in the east Iranian Makran. They fit tectonic reconstructions with Middle Jurassic intracontinental rift, Early Cretaceous to Eocene subduction below Central Iran forming a continental arc to the north of Makran and closure of the related oceanic in the Paleogene. Erosional products of the corresponding magmatic arc are found in the Makran Basin. Our data disprove that provenance characteristics of the Makran sedimentary rocks are consistent with derivation from the Himalayan sources.

Key words: West Makran, provenance analysis, detrital zircon, Hf isotopes, tectonic setting.

INTRODUCTION

The Makran Accretionary Wedge extends ~ 900 km along strike between SE Iran and SW Pakistan (fig. 1; White and Klitgord, 1976; White, 1982; Platt and others, 1985). The wedge, from rear to toe, is about 350 km wide along the nearly N-S convergence direction between Arabia and Eurasia (McCall and Kidd, 1982; DeMets and others, 2010) and grows both vertically and laterally by scraping sediments off the northwards subducting Arabian lithosphere (Platt and others, 1985). Northward subduction of the Arabian plate beneath the Central Iran and Afghan blocks started during the Cretaceous (for example McCall, 1997). The current subduction rate estimated by GPS measurements is about 2 cm/yr (Vigny and others, 2006; Masson and others, 2007). The accretionary wedge is divided into a 100 to 150 km wide active submarine wedge, to the south and the 200 to 250 km wide northern, onshore wedge (fig. 1). These two parts are separated by the coastal belt where onshore and offshore normal faults and mud volcanoes are prominent (McCall, 1983; Von Rad and others, 2000; Ellouz-Zimmermann and others, 2007b; Grando and McClay, 2007). The Paleogene sediments are supposedly supplied from the Himalaya via the Paleo-Indus River, while reworking of the growing accretionary wedge supplied sediments to the Miocene and

* Department of Earth Sciences, ETH Zurich, Sonneggstrasse 5, 8092, Zurich, Switzerland
† Corresponding author: ali.mohammadi@erdw.ethz.ch

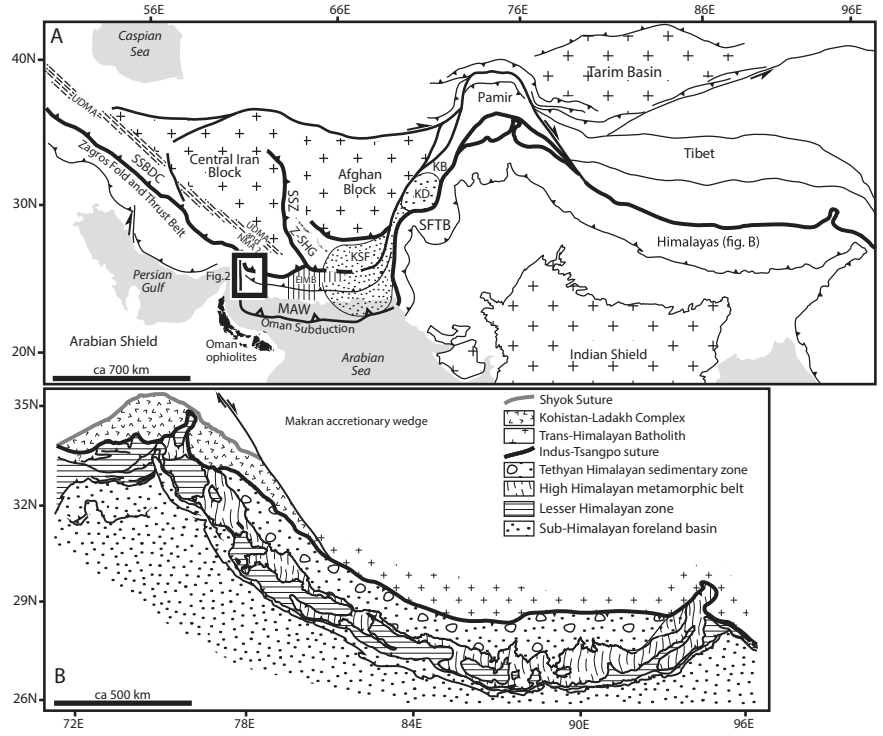

Fig. 1. (A) Simplified tectonic map of the potential source terranes: Abbreviations: EIMB: East Iranian Makran Basin; KB: Katawaz Basin; KD: Katawaz Delta; KSF: Khojak Submarine Fan; MAW: Makran Accretionary Wedge; NMA: North Makran Arc; SFTB: Sulaiman Fold-and-Thrust Belt; SSBDC: Sanandaj-Sirjan/Bajgan-Durkan Complexes; SSZ: Sistan Suture Zone; UDMA: Urmia-Dokhtar Magmatic Arc; Z-SHG: Zahedan- Shah kuh Granite; Framed area = study area mapped in fig. 2. (B) Simplified tectonic map of the South Tibet-Himalayan regions with potential sources discussed in the text.

more recent Makran deposits (fig. 1; Critelli and others, 1990; Qayyum and others, 1997b; Qayyum and others, 2001; Grigsby and others, 2004; Ellouz-Zimmermann and others, 2007a; Ellouz-Zimmermann and others, 2007b; Carter and others, 2010; Kassi and others, 2013). However, Mohammadi (ms, 2015) argued that detrital zircon U-Pb geochronology and provenance study of Late Cretaceous-Miocene sandstones of Iranian onshore Makran are better attributed to a nearby complex of ophiolites and a continental magmatic arc, to the north of the Makran Basin.

This work aims at further documenting the Late Mesozoic-Cenozoic sedimentary framework of the West Makran Basin in Iran (fig. 1), by investigating the provenance of siliciclastic sandstones. We combine fieldwork, modal framework grain compositions and heavy mineral analysis to characterize the lithologies eroded in the source areas and constrain the tectonic setting of the Makran Basin. More than two thousand U-Pb ages of detrital zircon obtained by laser ablation ICP-MS are used to evaluate crystallization ages of the source rocks. *In-situ* Hf isotope ratios of two hundred and four dated zircon grains allow inferring the origin of magmas in the source region.

GEOLOGICAL SETTING OF STUDIED SANDSTONES

The eastern part of the onshore Iranian Makran has been divided into four major east-west-oriented tectono-stratigraphic units separated by major thrust zones (Dolati, ms, 2010; Burg and others, 2013). Of these four units, only the North Makran (to the north) and the Coastal Makran (to the south) are present in Western Makran (fig. 2).

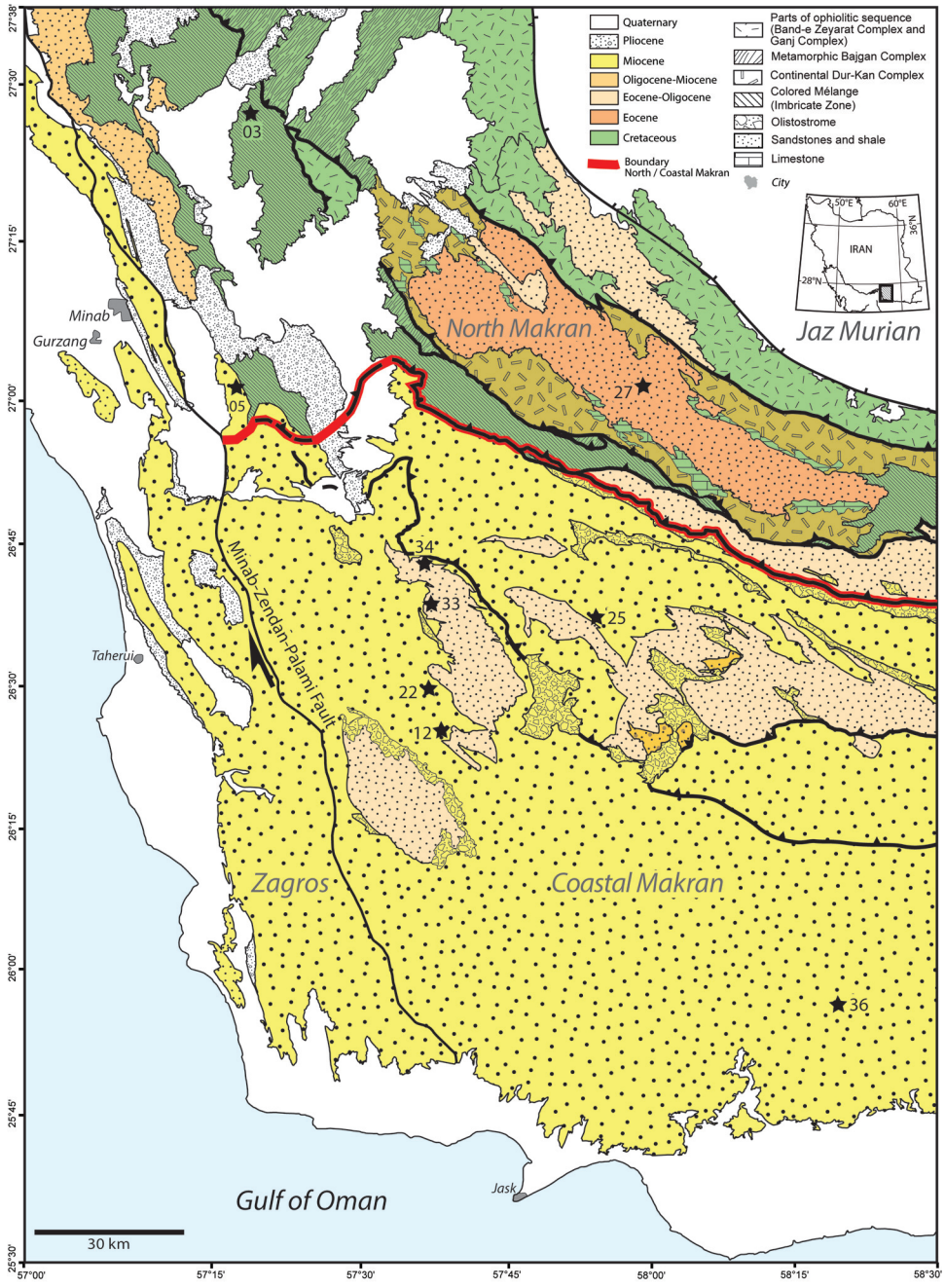

Fig. 2. Simplified geologic map of the West Makran Basin and Zagros. Stratigraphic ages according to the 1:250,000 geological maps of Bandar Abbas, Minab, Taherui and 1:100,000 geological maps of Jask-Gattan and Gabric (Samimi Namin and others, 1982; Samimi Namin and others, 1983; Fakhri, 1994; Samadian and others, 1999; Samadian and Khan Nazer, 1999).

North Makran

North Makran is widely exposed in the Fannuj and Minab quadrangle maps (McCall, 1985a, 1985b, 1985c, 1985d). It is divided into two major subunits: (1) in the north, ophiolitic mafic and ultramafic rocks with their upper crustal pillow lavas and Cretaceous deep-marine radiolarites and turbidites; these rocks were eroded and unconformably covered by Upper Cretaceous-Paleocene shallow water sediments, in turn unconformably covered by Eocene turbidites (Hunziker, 2014; fig. 2), (2) a tectonic imbricate (so-called colored mélange) consists of tectonic slices of subunit (1) and remnant continental units with granitoids and shallow water Permian-Jurassic carbonates (the Bajgan-Dur Kan zone of McCall and Kidd, 1982). The paleo-trench and related accreted sediments are exposed in the East Makran (Dolati, ms, 2010) but not exposed as a formal unit in the West Makran. Possibly some of the trench fill sediments were tectonically included in the imbricate zone (fig. 1). Eocene turbiditic shales, mudstones and sandstones with minor pelagic limestones are unconformable on the Imbricate Zone. They are comparable in lithological content and fossil ages to the proximal Eocene turbidites covering unconformably the North Makran Ophiolites (McCall, 1985c). This imbricate zone is thrust southward onto sedimentary sequences of the Makran Accretionary Wedge.

Coastal Makran

Coastal Makran, in Western Makran like further east, preserves a record of Miocene shelf carbonate rich mudstone/sandstone to Pliocene continental conglomerates filling up the basin to above sea level. Sporadic occurrences of deep-sea Eocene and Oligocene turbiditic sequences in anticlinal cores represent the underlying rocks. The Lower Miocene consists of poorly cemented rhythmic sequences of shale and carbonate-rich sandstones typifying a lower shelf environment. The Middle and Upper Miocene are divided into (1) a lower, marl-dominated and (2) a calcareous sandstone-dominated members. The marl-dominated member mainly consists of medium to very thick bedded marlstones with minor fine to medium grained and thin to medium bedded calcareous sandstones. Such shallowing upward para-sequences are typical for upper shelf environment. (fig. 2; Samimi Namin and others, 1982; Samadian and others, 1999; Samadian and Khan Nazer, 1999).

METHODS

The studied western part of the Iranian Makran (fig. 1) is covered by the Minab and Taherui 1:250,000 geological maps (Samimi Namin and others, 1982; Samimi Namin and others, 1983) and Jask-Gattan and Gabric 1:100,000 geological maps (fig. 2; Samadian and others, 1999; Samadian and Khan Nazer, 1999). These maps and associated reports, subdivide the turbiditic and shelf sequences into six, several hundred meters thick lithostratigraphic units (Samimi Namin and others, 1982; Samimi Namin and others, 1983; Samadian and others, 1999; Samadian and Khan Nazer, 1999). Nine medium-grained turbiditic sandstones (with prefix 15AM in the ETH collection) have been studied (fig. 2 and table S1; http://earth.geology.yale.edu/%7eajs/SupplementaryData/2017/Mohammadi/TableS1.xlsx). Samples of hemipelagic sediments were taken to avoid reworked nannofossils in stratigraphic determinations. These nannofossil samples confirmed the published stratigraphy, with sedimentation ages ranging from Late Cretaceous to Miocene. Mineral separation, mineral identification techniques, and analytical methods are described in Appendix I.

RESULTS

Paleocurrent Indicators

Measured paleocurrent directions obtained from flute casts and asymmetric ripples in Oligocene and Miocene turbiditic sequences were rotated to horizontal

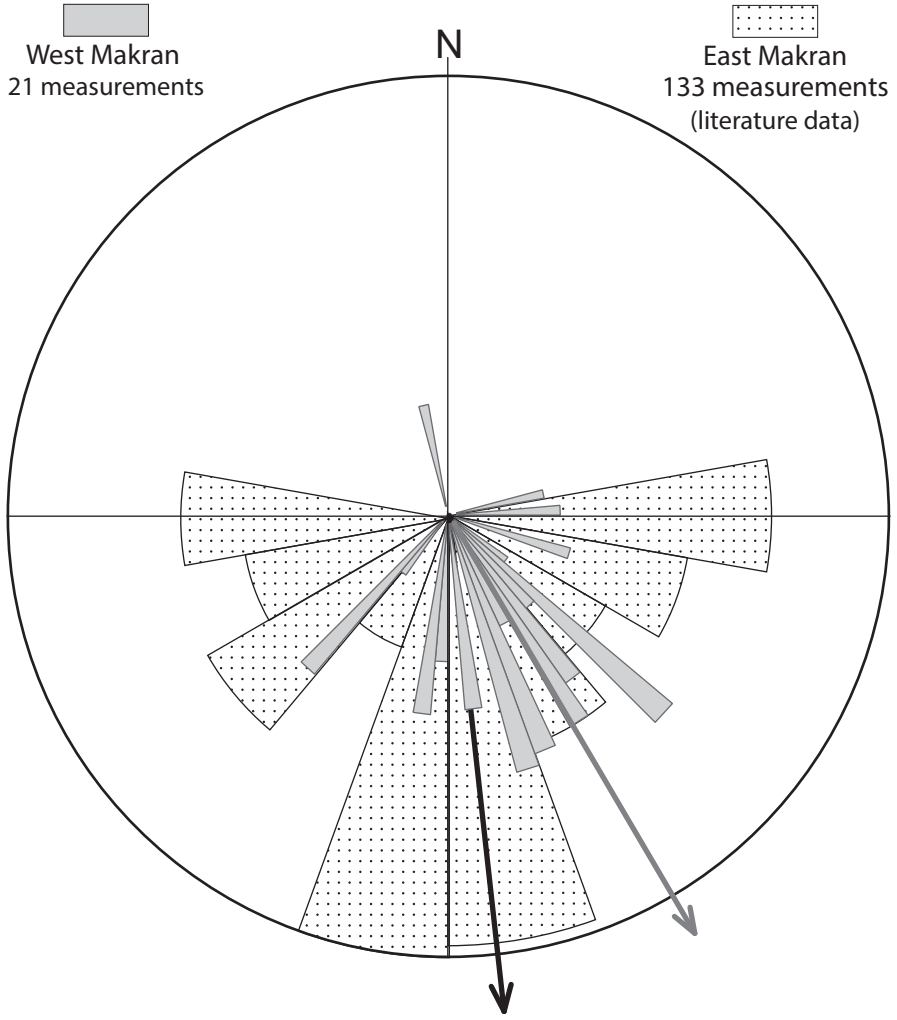

Fig. 3. Rose diagrams of paleocurrent measurements: 5 asymmetric ripple marks and 16 flute casts in Western Makran. Literature data from Miocene strata paleocurrent of East Makran from Mohammadi and others (2016c). Results restored to horizontal around the local strike of bedding. Arrows: average directions.

around the local strike direction of bedding and plotted in rose diagrams. They indicate average paleoslope and flow direction from NW to SE (fig. 3). This direction slightly differs from, but remains grossly consistent with paleocurrent measurements in the eastern Iranian Makran (fig. 3).

Modal Sandstone Composition

West Makran sandstones are mainly classified as feldspathic litharenite and litharenite (fig. 4A). Feldspar is dominantly plagioclase (>90%) with minor amounts of K-feldspar; quartz grains are mostly mono-crystalline (80%) (fig. 4B and table S2, http://earth.geology.yale.edu/%7eajs/SupplementaryData/2017/Mohammadi/TableS2.xlsx). Rock fragments are mostly sedimentary and volcanic lithics, few are metamorphic (figs. 4C and 4D). Andesite and volcanic glass are dominant among

the volcanic rock fragments. Sedimentary lithic fragments include limestone, dolomite and siltstone. Metamorphic rock fragments generally consist of foliated polycrystalline quartz and low-grade to medium-grade phyllites, and schists (figs. 4C and 4D). In Late Cretaceous sandstone (sample 15AM03) muscovite and biotite are abundant and rock fragments are dominantly metamorphic lithic grains (> 45%; table S2, http://earth.geology.yale.edu/%7eajs/SupplementaryData/2017/Mohammadi/TableS2.xlsx).

Heavy Minerals

The heavy mineral spectrum indicates very variable compositions, which can be subdivided into four main groups: (1) Most stable minerals (zircon, monazite, tourmaline, rutile, anatase and brookite; ZTR = 7 – 57%) and apatite, which are likely derived from continental crust sources. (2) Less stable minerals (garnet, epidotes, andalusite, staurolite, kyanite, chloritoid) in variable amounts (2 – 63% of total grain count) suggesting metamorphic rocks in the source area. (3) Cr-spinel (up to 27% of total grain count) indicating contribution from exhumed ultramafic rocks. (4) Pyroxenes (enstatite, diopside, ferrosilite and hedenbergite) from intermediate to basic magmatic rocks (fig. 5 and table S3, http://earth.geology.yale.edu/%7eajs/SupplementaryData/2017/Mohammadi/TableS3.xlsx). Middle-Upper Eocene sandstone (sample 27) generally yielded large amounts (up to 89% of total grain count) of pyroxenes. Middle Miocene sandstone (sample 05) show large amounts (up to 45% of total grain count) of garnet (fig. 5 and table S3, http://earth.geology.yale.edu/%7eajs/SupplementaryData/2017/Mohammadi/TableS3.xlsx).

Detrital Zircon Dating and Hf Isotope Ratio

LA-ICPMS U-Pb dating was performed on 2307 detrital zircons of eight Eocene-Miocene sandstone samples (figs. 6, 7, 8 and table S4, http://earth.geology.yale.edu/%7eajs/SupplementaryData/2017/Mohammadi/TableS4.xlsx). Euhedral to subhedral shapes of these grains (80%), suggest short transport distances from source to sink. Owing to the importance of the youngest crystallization age of zircons for provenance studies, we dated rims only. Obtained ages range between 3.3 Ga and 18 Ma, with four main peaks around 165, 95, 89 and 48 Ma and a minor peak around 22 Ma. Due to their rarity, zircons older than 1100 Ma were not plotted in figures 6, 7 and 8. We also did not plot ages with discordance greater than 10 percent. Like in the East Iranian Makran Basin zero to very short lag times (that is, Eocene zircons hosted in sandstone of similar stratigraphic age) indicates syn-sedimentary magmatism in the source area (fig. 9; Mohammadi and others, 2016c).

Depending on the texture (that is, inclusions and internal growth structure imaged by backscattered-electron and cathodoluminescence) and size of the zircon grains, *in-situ* Hf isotope ratios were measured on dated zircons. Measurements on 204 analytical spots yield $\varepsilon\text{-Hf}_{(t)}$ values from −16.5 to +19.9. Late Cretaceous zircon grains show a large variation in $\varepsilon\text{-Hf}_{(t)}$, from −11.8 to +19.1 most of them being between $\varepsilon\text{-Hf}_{(t)} = 0$ and +13. Zircons with Eocene ages have $\varepsilon\text{-Hf}_{(t)}$ value between +14.5 and −5.9, a large majority between 0 and +12 and few with negative values (fig. 10 and table S5, http://earth.geology.yale.edu/%7eajs/SupplementaryData/2017/Mohammadi/TableS5.xlsx). Compared to the Late Cretaceous zircons, Eocene zircons show less positive $\varepsilon\text{-Hf}_{(t)}$ between the chondrite union reservoirs (CHUR) and depleted mantle lines (fig. 10). Positive $\varepsilon\text{-Hf}_{(t)}$ values indicate depleted mantle signatures while the negative $\varepsilon\text{-Hf}_{(t)}$ indicate magmatic zircons with continental-crust derived melts or mixed depleted mantle derived melts with old crustal component signature (for example Patchett, 1983; Yuan and others, 2008).

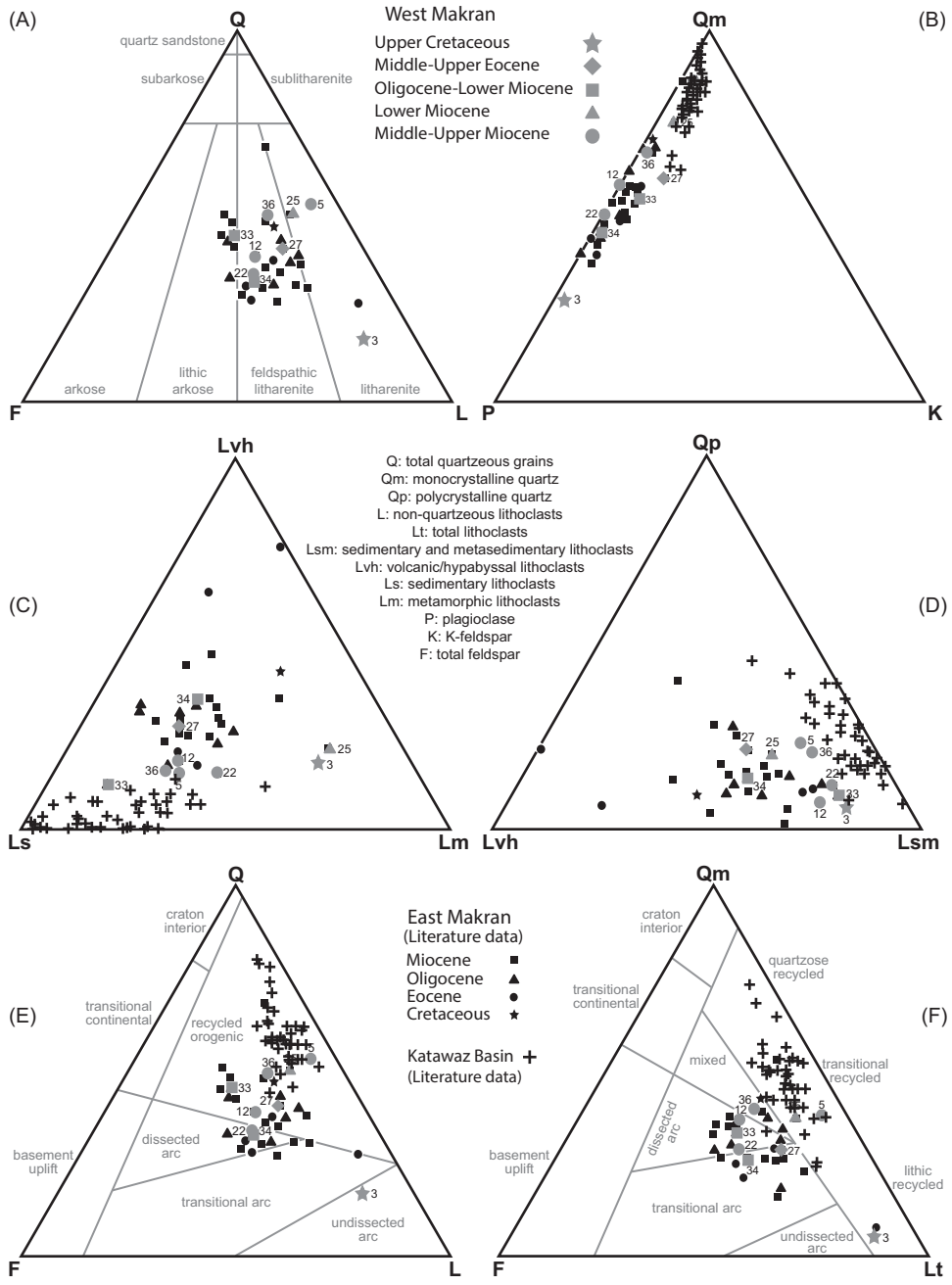

Fig. 4. Detrital composition and classification in provenance discrimination diagrams West Makran sandstones: (A) sandstone classification diagram (Folk, 1980); (B) Qm-P-K diagram after (Dickinson and Suczek, 1979); (C) Lvh-Ls-Lm diagram after (Dickinson, 1985); (D) Qp-Lvh-Lsm diagram after (Dickinson and Suczek, 1979); (E) QFL (Dickinson, 1985) and (F) QmFLt (Dickinson, 1985). Literature data from Late Cretaceous-Miocene strata of East Makran from Mohammadi and others (2016c) and Middle Eocene-Early Miocene Khojak formation in Katawaz Basin from Qayyum and others (2001).

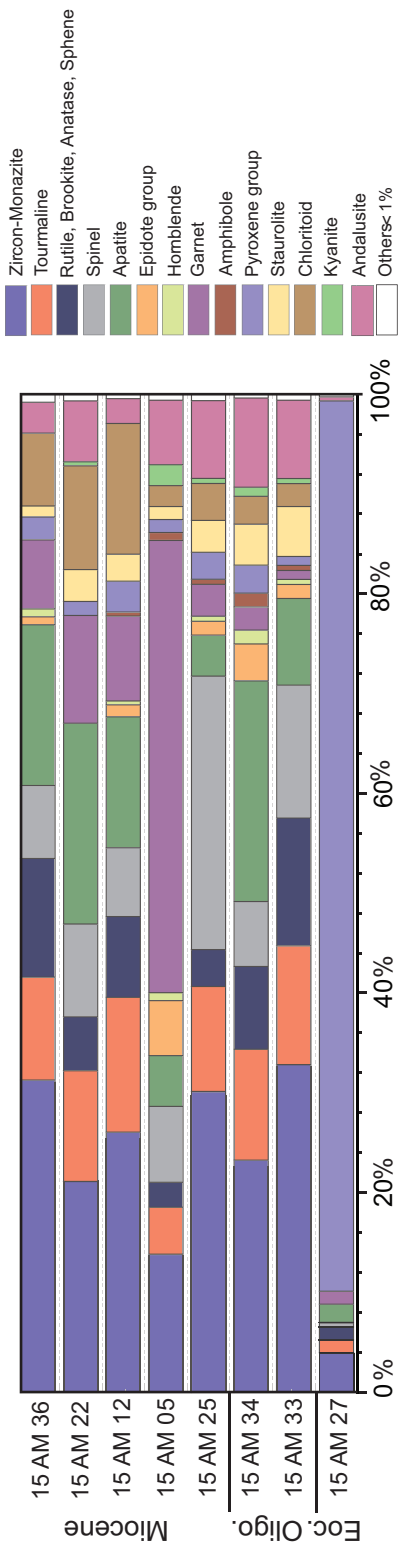

Fig. 5. Heavy mineral assemblages showing the relative abundance of heavy mineral species. West Makran sandstones arranged in reconstructed stratigraphical order.

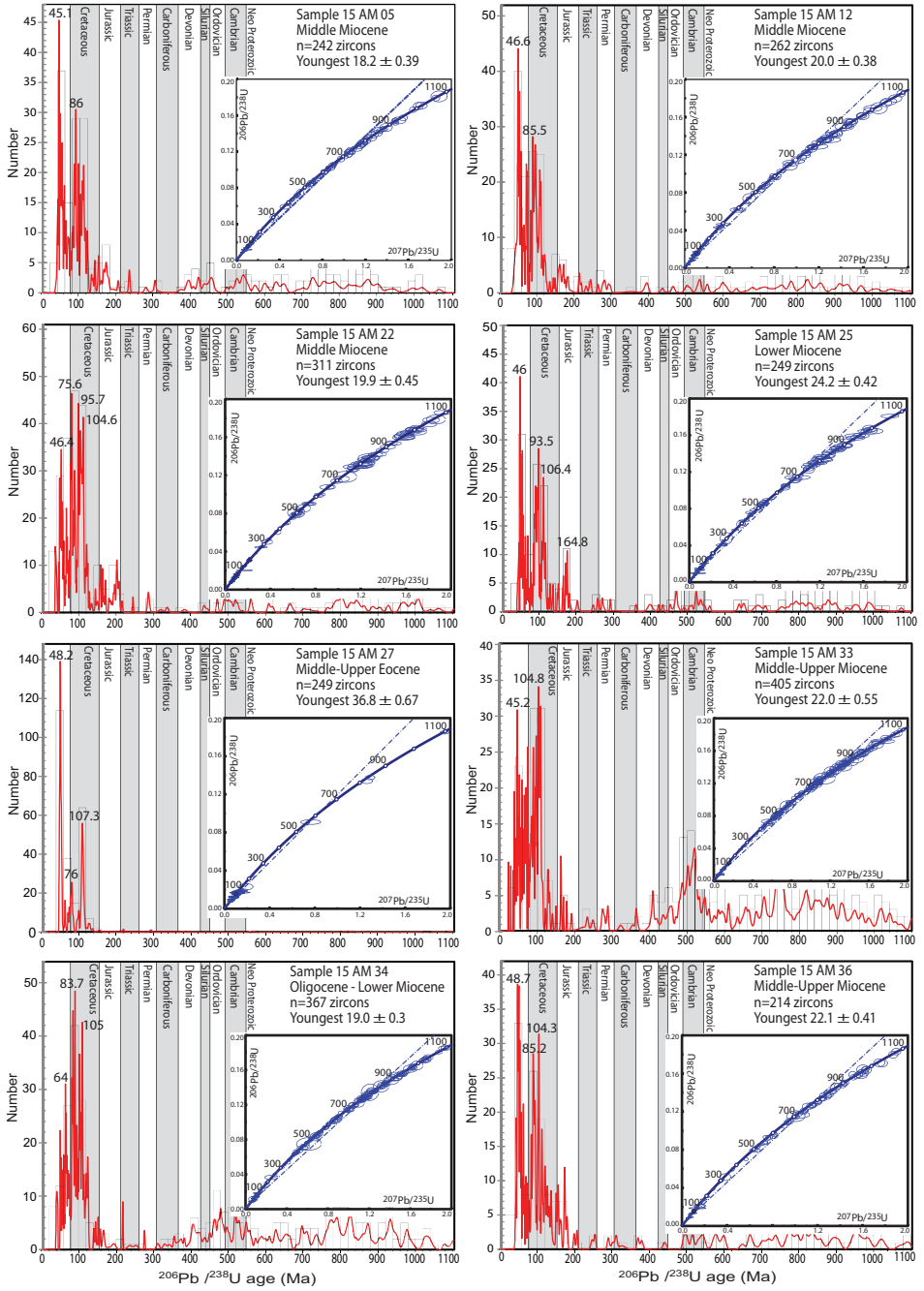

Fig. 6. Detrital zircon $^{206}Pb/^{238}U$ age population probability density diagrams with corresponding Concordia plots of concordant detrital zircons of the samples 05, 12, 22, 25, 27, 33, 34 and 36 from West Makran sandstones. Discordance zircon ages (greater than 10%) are not included. Time scale after Gradstein and others (2012).

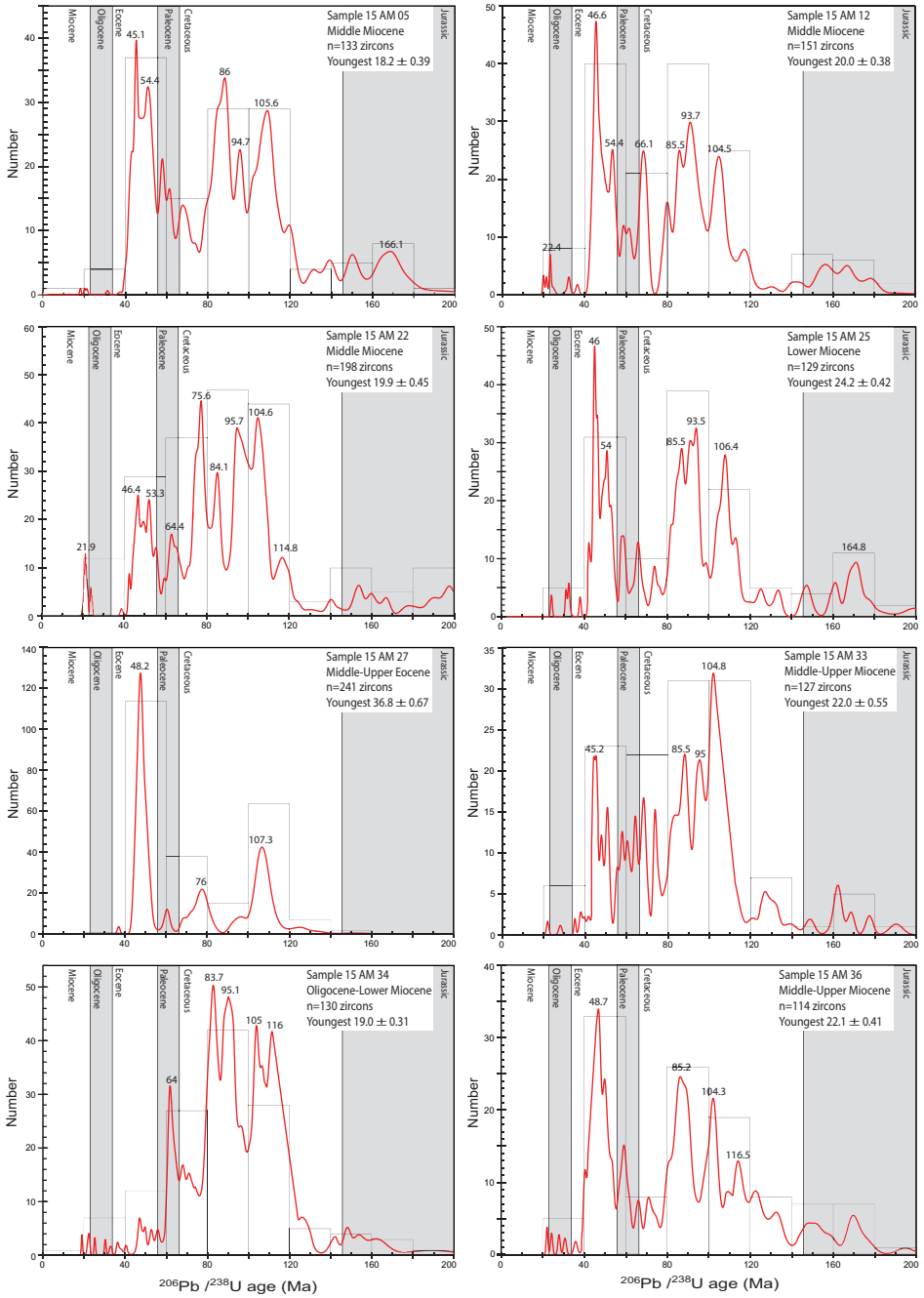

Fig. 7. Detrital zircon $^{206}Pb/^{238}U$ age population probability density diagrams for 0-200 Ma of the samples 05, 12, 22, 25, 27, 33, 34 and 36 from West Makran sandstones. Time scale after Gradstein and others (2012).

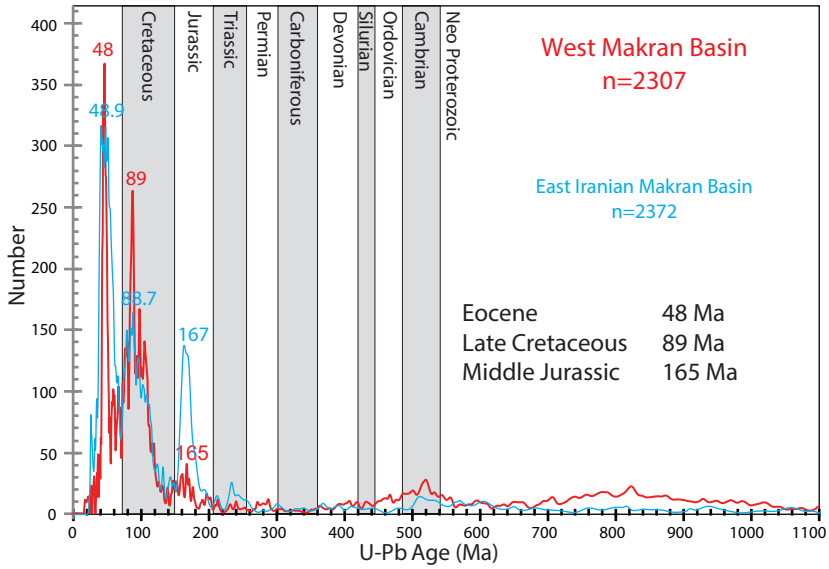

Fig. 8. Zircon U-Pb age distribution pattern of West Makran sandstone samples. Time scale after Gradstein and others (2012). Literature data from Late Cretaceous-Miocene strata of East Makran from Mohammadi and others (2016c).

DISCUSSION

Taken together the new U-Pb geochronology and *in-situ* Hf isotope data of detrital zircons, heavy mineral and sandstone framework compositions of the Late Cretaceous-

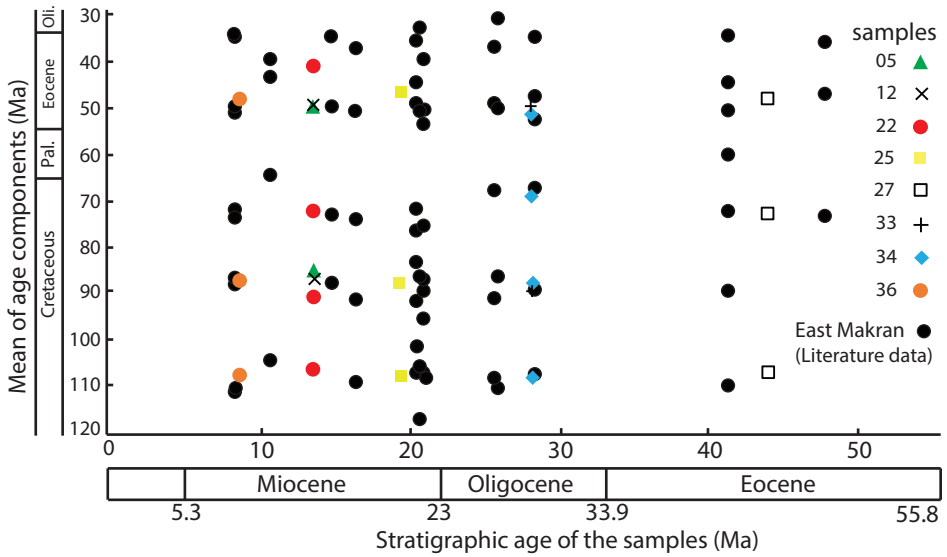

Fig. 9. West Makran sandstones stratigraphic age versus detrital zircon mean U-Pb age populations. Time scale after Gradstein and others (2012). Literature data from Eocene-Miocene strata of East Makran from Mohammadi and others (2016c).

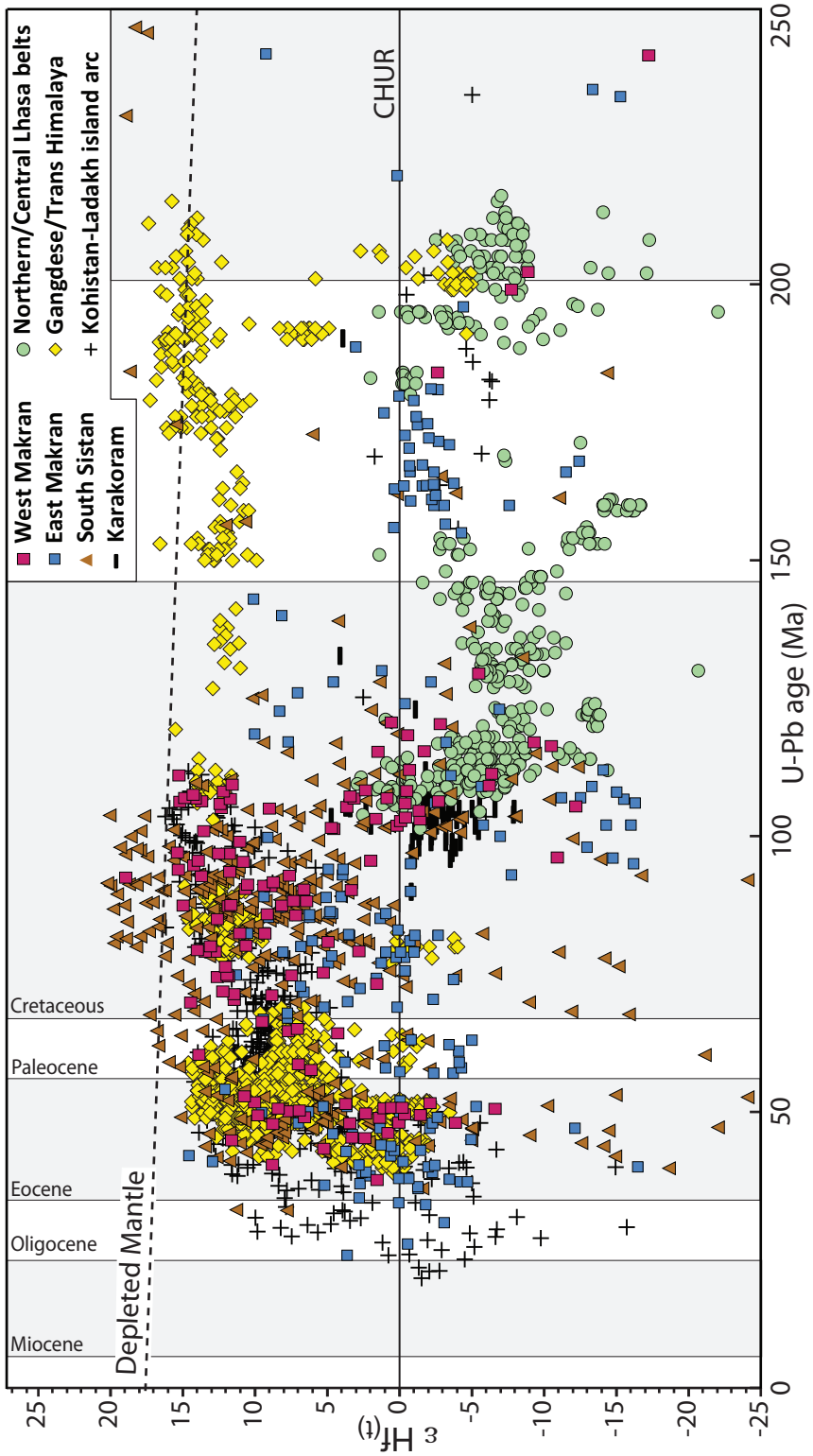

Fig. 10. Time-corrected $\varepsilon Hf_{(t)}$ values versus of West Makran detrital zircon $^{206}U/^{238}Pb$ ages (Ma) and published $\varepsilon Hf_{(t)}$ data of East Makran and South Sistan sandstones (Mohammadi and others, 2016b; Mohammadi and others, 2016c), Karakoram batholith, Gangdese-Trans Himalaya and Indus Molasse, northern-central Lhasa belt and Kohistan-Ladakh arc, (Heuberger and others, 2007; Wu and others, 2007; Ji and others, 2009; Bouilhol and others, 2013; Zhuang and others, 2015). Depleted Mantle evolution trend (dashed line) from Griffin and others (2000) and Chondritic Uniform Reservoir values (CHUR) from Blichert-Toft and Albarède (1997). The evolved epsilon hafnium ($\varepsilon Hf_{(t)}$) data from zircons older than 250 Ma are not shown. Time scale after Gradstein and others (2012).

Miocene sandstones of West Makran and comparison with published data on the eastern part of Iranian Makran (Mohammadi and others, 2016c) refine our understanding of the tectonic setting and sources of the Makran turbiditic basin.

Sandstone Framework Analysis

The modal frameworks show that West Makran sandstones are largely composed of volcanic lithic and sedimentary fragments with subordinate metamorphic lithics. Such an association is consistent with main provenance from a magmatic arc (transitional-dissected arc during the Eocene-Oligocene; figs. 4C and 4D) and recycled orogenic terranes in the Miocene (figs. 4E and 4F). The only Late Cretaceous sandstone (sample 15AM03) is dominated by metamorphic lithic grains, presumably collecting detritus from the proximal Bajgan metamorphic belt (fig. 2). In ternary QFL diagram, the framework compositions shift from the Q-L binary in Eocene-Oligocene sandstones toward slightly quartz-richer compositions in Miocene sandstones (fig. 4A). The recycled orogenic nature of the source area (accreted Late Cretaceous-Oligocene sediments) is characterized by the slight increase in quartz amount in some Miocene sandstones (figs. 4E and 4F). A similar modal framework composition and provenance setting was reported for the Eocene to Miocene sandstones of the east Iranian Makran (fig. 4; Mohammadi and others, 2016c).

Heavy Mineral Assemblage

Like the sandstone framework, the heavy mineral assemblages indicate that the West Makran sandstones contain typical elements of a magmatic arcs system, ophiolites (Cr-spinel and rare serpentinite) and metamorphic suites: (1) arc volcanism is clear from the andesitic and volcanic glass lithic components along with pyroxenes and feldspars. (2) Epidote and pyroxene may have been originated from exhumed ophiolites, metamorphic rocks or mafic to intermediate intrusive rocks (fig. 5). The amount of pyroxene is significantly high (89.2%), while the amount of Cr-spinel decreases in Eocene sandstone (sample 15AM27). This implies that intermediate to mafic magmatic-volcanic rocks became at least more eroded than the ultramafic sources in Eocene times. Sample 15AM27 was taken from the local basin within an imbricate zone (fig. 2). (3) Abundant metastable heavy minerals such as garnet, staurolite, chloritoid, and metamorphic lithic grains represent metamorphic rocks as subsidiary sources (Deer and others, 1992), which may have formed either within the arc crust or in the accretionary wedge of the time. The heavy mineral spectrums of the West Makran and eastern part of Iranian Makran are similar, except blue amphibole (glaucophane) which is absent in the West Makran sequence (Mohammadi and others, 2016c).

Detrital Zircons U-Pb Age and In-situ Hf Isotopes

U-Pb ages of West Makran detrital zircon are between ca. 3.3 Ga and ca. 31 Ma (figs. 6, 7, 8, 9 and table 1). Four U-Pb age groups are identified.

The first group includes zircon grains dated from Archean (3.3 Ga) to earliest Jurassic (200 Ma). Archean (3.3 Ga) is the oldest zircon age reported from Makran Basin. This range in ages creates a broad heterogeneous spectrum in which Neoproterozoic-Cambrian zircons (1000 – 460 Ma) are more abundant (table S4, http://earth.geology.yale.edu/%7eajs/SupplementaryData/2017/Mohammadi/TableS4.xlsx). Detrital zircons of this spectrum are distributed into two subgroups: 1) the rounded and anhedral zircon grains without internal growth zoning are either fragments or old zircons reworked from continental crystalline rocks or inherited magmatic zircons. Their origin is uncertain. The location of possible igneous/metamorphic source is undefined, due to the likelihood of repeated reworking through several tectonic cycles since the Archean. Restricting conjecture to the closest continental block and southward paleocurrent directions points to the

TABLE 1

Compilation of provenance indicators from magmatic arcs and contemporaneous sedimentary basins in the Himalayan system, Makran accretionary wedge, south Sistan basin and Oman ophiolite belt

Potential sources area	Zircon U-Pb age		Hf isotope composition		Sandstone framework (dominant lithics)	Heavy minerals	References
	Main peaks (Ma)	Minor peaks (Ma)	Age	ε-Hf$_{(t)}$			
West Makran Basin	165; 108; 89 and 48	550-1000	Late Cretaceous Eocene	-11.8 to +19.1 -5.9 to +14.5	volcanic and sedimentary	ZTR+apatite ≥ 69%, Cr-spinel, lack of blue amphibole	This study
East Iranian Makran Basin	166.5; 88.7 and 48.9	563-868	Middle Jurassic Early Cretaceous Late Cretaceous-Eocene	-13 to +2 -17 to +11 -6 to +14	volcanic and sedimentary	ZTR+apatite ≥ 75%, Cr-spinel, Blue amphibole	[1]
Sistan Suture Zone	89 and 49.5	-	Cretaceous Eocene	-17 to +20.4 -24 to +16	volcanic and sedimentary	ZTR+apatite ≥ 81%, Cr-spinel, Lack of blue amphibole	[2]
Katawaz Basin	58; 80 and 93	563-836	-	-	sedimentary and minor volcanic	-	[3]
Sulaiman Fold-and-Thrust Belt	42-47; 70; 83 and 98	490-960	-	-	metamorphic and sedimentary	ZTR + apatite (9-86%) Cr-spinel (0-17%)	[4]
Indus-Tsangpo Suture molasse	58 and 98	480-1250	-	-	volcanic and felsic plutonic	Lack of Cr-Spinel	[5]
Kailas Basin	24-26; 48 and 75-80	19.5% of detrital zircons >100 Ma	-	-	volcanic and sedimentary	Lack of Cr-Spinel	[6]
Karakoram batholith	18; 64 and 108	-	Cretaceous	-6.5 to +5	-	-	[7]
Kohistan-Ladakh Complex	58 and 98	-	Cretaceous Eocene	+6 to +17 -7.40 to +14	-	-	
Trans-Himalayan Batholith	46-65 and 80-103	-	Cretaceous Eocene	-4.7 to +15.3 -4.1 to +15	-	-	[8]
Zahedan-Shah Kuh plutonic belt	40.5-44.3 28.9-30.9	-	Eocene Oligocene	-7.13 to +8.54 -3.3 to +11.65	-	-	[9]
North Makran Jurassic granites	160-166.6	-	-	-	-	-	[10]
Oman ophiolite	91-98	-	-	-	-	-	[11]

[1]: (Mohammadi and others, 2016c); [2]: (Mohammadi and others, 2016b); [3]: (Carter and others, 2010); [4]: (Zhuang and others, 2015); [5]: (Henderson and others, 2010; Roddaz and others, 2011); [6]: (DeCelles and others, 2011); [7]: (Fraser and others, 2001; Honegger and others, 1982; Jain and Singh, 2008; Krol and others, 1996; Parrish and Tirrul, 1989; Phillips and others, 2004; Ravikant and others, 2009; Schaltegger and others, 2002; Schärer and others, 1984; Singh and others, 2007; Upadhyay and others, 2008; Weinberg and others, 2000); [8]: (Ji and others, 2009; Wen and others, 2008; Zhu and others, 2008); [9]: (Mohammadi and others, 2016a); [10]: (Hunziker and others, 2015) [11]: (Chen and Pallister, 1981; Rioux and others, 2012; Tilton and others, 1981; Warren and others, 2005).

nearby Central Iranian Block whose basement is composed of metamorphic and igneous rocks. Central Iran was deformed during the Late Precambrian and overprinted by younger igneous events (Nadimi, 2007). Consistently, zircon U-Pb ages of magmatic, metamorphic and siliciclastic rocks of this continental block span from 462 to 1870 Ma with few Archean zircon cores; the major population peak stands between 525 to 547 Ma (Ramezani and Tucker, 2003; Hassanzadeh and others, 2008). Detrital zircon ages of a single Cenozoic sandstone from the northern part of Central Iran reveal a main peak at 50 Ma and a secondary peak at 450 Ma (Horton and others, 2008). The reported Neoproterozoic-Ordovician detrital zircon ages are comparable to age spectra from the Central Iranian craton. 2) The second subgroup consists of very fine zircon grains (< 50 μ) with euhedral and magmatic zoning. Due to their size, cores and rims were mixed during laser ablation so that the last crystallization age is not ascertained.

The second zircon group is Jurassic, with the main peak at 165 Ma (figs. 6, 7, 8 and table S4, http://earth.geology.yale.edu/%7eajs/SupplementaryData/2017/Mohammadi/TableS4.xlsx). Considering the magmatic zoning, high Th/U ratios (0.8–8.9) and euhedral shapes ($\geq 60\%$), these zircons are attributed to igneous rocks. Jurassic (160–166.6 Ma) granitoids are actually known in North Makran; petrology, geochemistry and Rb-Sr as well as Nd-Sm isotopes suggest that these granitoids originated during extension/thinning and subsequent partial melting of a continental crust (Hunziker and others, 2015). Indeed, the negative $\varepsilon Nd_{(i)}$ and high initial Sr isotopic ratios are symptomatic of a significant crustal contribution to the melt. The rift setting is supported by field observation of North Makran granites that reached near-surface depths and intruded shelf limestones (Hunziker and others, 2015). Supportively also, the granophyric and perthitic texture of these granites is a common feature of granite intrusions in continental rifts (Coleman and others, 1992). This interpretation fits the negative ε-$Hf_{(t)}$values (-1.9 to -8.2) of the analyzed Middle Jurassic zircons in Western Makran (fig. 10 and table S5, http://earth.geology.yale.edu/%7eajs/SupplementaryData/2017/Mohammadi/TableS5.xlsx).

The third group includes detrital zircons of Late Cretaceous age (115–66 Ma with main peaks at 105 Ma, 95 Ma, 89 Ma, 75 Ma, and 66 Ma; figs. 6, 7, 8 and table S4, http://earth.geology.yale.edu/%7eajs/SupplementaryData/2017/Mohammadi/TableS4.xlsx). The euhedral shape and magmatic zoning of most grains ($>70\%$), and generally high Th and U contents with $Th/U > 1$, suggest proximal Upper Cretaceous magmatic source. The large range in ε-$Hf_{(t)}$ values (-11.5 to $+19.1$, in majority between 0 and $+13$; fig. 10 and table S5, http://earth.geology.yale.edu/%7eajs/SupplementaryData/2017/Mohammadi/TableS5.xlsx) represents positive and negative ε-$Hf_{(t)}$ values indicating non-depleted mantle and continental crust signatures as can be expected for subduction-related magmatism in continental arcs (for example Patchett, 1983; Yuan and others, 2008; Naing and others, 2014).

The fourth group contains zircons from 60 to 36 Ma with peak at 48 Ma (figs. 6, 7, 8 and table S4, http://earth.geology.yale.edu/%7eajs/SupplementaryData/2017/Mohammadi/TableS4.xlsx). Euhedral shapes ($>85\%$) suggests a short distance between source and sink. The wide range in Th and U, and $Th/U > 1$, and internal structures (magmatic zoning) of zircons, indicate a magmatic origin. The variable εHf values ($+14.5$ and -5.9, a large majority between 0 and $+12$; fig. 10 and table S5, http://earth.geology.yale.edu/%7eajs/SupplementaryData/2017/Mohammadi/TableS5.xlsx), indicate non-depleted mantle signatures (positive ε-$Hf_{(t)}$ values) with juvenile input from molten felsic rocks (negative ε-$Hf_{(t)}$ values) as expected in a continental arc (for example Patchett, 1983; Blichert-Toft and Albarède, 1997; Vervoort and Blichert-Toft, 1999; Naing and others, 2014).

The Urmia-Dokhtar Magmatic Arc (UDMA, fig. 1) is a continental arc attributed to subduction during convergence between the Arabian and Eurasian plates (Şengör

and others, 1988). The andesites and basalts of this arc yield two age intervals: Late Cretaceous (81–72 Ma) and Middle Eocene-Late Miocene (45–6 Ma; Chiu and others, 2013). The main Late Cretaceous (105 Ma, 95 Ma, 89 Ma, 66 Ma) and Eocene (48 Ma) peaks measured on clastic zircons in west Makran sandstones are not known in UDMA. Therefore, the Makran detritus is not derived from this arc. Instead, Makran sediments represent a "lost" Late Cretaceous-Eocene North Makran Magmatic Arc produced by northward subduction beneath Central Iranian Block of the North Makran oceanic basin, now represented by the North Makran ophiolites, (McCall, 1995; Hunziker and others, 2015).

The fifth zircon group is Early Miocene, with the main peak at 22 Ma (figs. 6, 7 and table S4, http://earth.geology.yale.edu/%7eajs/SupplementaryData/2017/Mohammadi/TableS4.xlsx). This group contains 19 out of 2300 detrital zircon grains. These Miocene zircons have euhedral shapes, which suggests a magmatic source not far from the deposition site. Their small size ($< 40\mu$) prevented performing Hf isotopic analysis. Early Miocene Ar-Ar age (22–18 Ma) were measured on UDMA basalts and rhyolites (Chiu and others, 2013), which may have been the source of these Miocene clastic zircons.

Potential Source Areas

Previous hypotheses suggested that the Paleo-Indus delta-submarine fan in the Katawaz Basin (fig. 1) supplied Himalayan sediments, which were transported further westward into the "Khojak" submarine fan and the Makran Basin (Critelli and others, 1990; Qayyum and others, 1997a; Qayyum and others, 2001; Grigsby and others, 2004; Ellouz-Zimmermann and others, 2007a; Ellouz-Zimmermann and others, 2007b; Carter and others, 2010; Kassi and others, 2011; Kassi and others, 2013; Kassi and others, 2015). This interpretation does not fit the data which, for comparison, are summarized in table 1.

The Late Eocene to Early Miocene sandstones of the Katawaz Basin contain abundant sedimentary lithic grains (siltstone, fine grained sandstone) with subordinate amounts of low-grade metamorphic clasts and few volcanic lithic fragments (figs. 4B, 4C, 4D and table 1; Qayyum and others, 1996). The recycled orogenic composition of these sandstones (figs. 4C, 4E and 4F) contrasts with the abundance of volcanic lithic grains, high ratio of volcanic lithic/metamorphic lithic and magmatic arc provenance in West Makran sandstones. Moreover, the Eocene detrital zircon grains (48 Ma) of West Makran are almost absent in Katawaz sandstone sequences (fig. 11 and table 1). Therefore, sediments of the Katawaz Basin were not recycled into the studied West Makran.

Similarly, a mixed orogenic provenance with a major contribution from the Tethys Himalaya, Karakorum and subordinate contributions from the ophiolitic Suture and Trans-Himalaya were suggested for the deposits in the Sulaiman fold-and-thrust belt (Roddaz and others, 2011; fig. 1). Zircon and apatite are almost absent in the Early Oligocene sandstones of the Sulaiman fold-and-thrust belt (Roddaz and others, 2011), while zircon and apatite together constitute 25 to 48 percent of the total heavy mineral assemblages in West Makran sandstones. The Sulaiman Paleocene-Middle Miocene strata contain Neoproterozoic detrital zircon (>90%) and minor amounts of zircons are younger than 100 Ma (<10%), whereas in the West Makran, zircon grains younger than 100 Ma are dominant (fig. 11 and table 1). We conclude that the West Makran and the Sulaiman fold-and-thrust belt had separate source regions during the Oligocene.

Comparison of the new detrital zircon U-Pb ages and Hf isotopic compositions of the West Makran with those from Himalayan regions [the Indus Suture molasses, the Kailas Basin, the Karakoram and Kohistan-Ladakh Arc, the Trans-Himalaya (Gangdese) batholith, fig. 1B] and other potential sources such as South Sistan Basin and

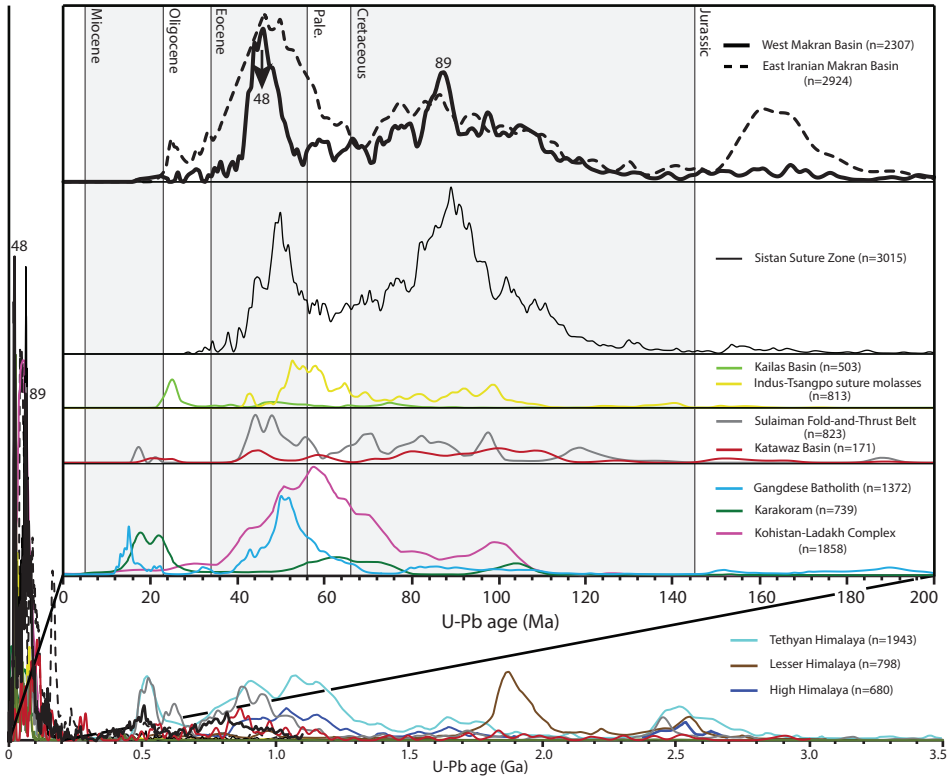

Fig. 11. Detrital and magmatic zircon U-Pb age probability plots of: West Makran strata, East Makran and South Sistan Basins (Mohammadi and others, 2016b; Mohammadi and others, 2016c), Indus Suture molasses (Henderson and others, 2010), Kailas Basin (DeCelles and others, 2011), Sulaiman Fold-and-Thrust Belt (Zhuang and others, 2015), Katawaz Basin (Carter and others, 2010), Gangdese Batholith (Chu and others, 2006; Wen and others, 2008; Ji and others, 2009), Karakoram Batholith and Kohistan-Ladakh Arc (Honegger and others, 1982; Schärer and others, 1984; Parrish and Tirrul, 1989; Krol and others, 1996; Weinberg and Dunlap, 2000; Fraser and others, 2001; Schaltegger and others, 2003; Phillips and others, 2004; Singh and others, 2007; Jain and Singh, 2008; Upadhyay and others, 2008; Ravikant and others, 2009), Tethyan Himalayan strata, Lesser Himalayan strata and Higher Himalayan strata (for example Gehrels and others, 2011).

Zahedan-Shah Kuh plutonic belt in SE Iran and Oman (Semail) ophiolite (fig. 1), further challenges the Paleo-Indus delta-submarine fan hypothesis and strengthens the concept of detritus source from a Mesozoic-Cenozoic North Makran continental arc and ophiolitic rocks. To summarize, the Lesser and High Himalayas (fig. 1B) were not exposed before the Early Miocene (for example DeCelles and others, 2000). Therefore, the West Makran sediments cannot contain detritus from these regions. Detrital zircon U-Pb age clusters from the Tethyan Himalayan sedimentary sequences and Indus Suture molasses differ from ages in the West Makran strata (fig. 11 and table 1). In particular, the Late Cretaceous (108 Ma and 89 Ma) main peak of West Makran zircons is almost absent in Kailas sequences (fig. 11 and table 1). Zircon ages distribution pattern and Hf isotopic composition in West Makran Basin is different than both Karakoram batholith and Kohistan-Ladakh arc (figs. 10, 11 and table 1). The Late Cretaceous (89 Ma) main peak of West Makran zircons is almost absent in the Trans-Himalaya (Gangdese batholith; fig. 11 and table 1). In addition, Hf isotopic values from the Trans-Himalaya are more positive than the Hf isotopic values recorded

in the West Makran zircons. ε-$Hf_{(t)}$ values of Trans-Himalayan Cretaceous zircons are also more positive than those of west Makran Cretaceous zircons. Such values define a mantle signature in Trans Himalaya while ε-$Hf_{(t)}$ values of west Makran zircons define a continental magmatic arc signature (fig. 10 and table 1). Hence, the West Makran detritus were not supplied from the Himalayan belts.

Considering sources closer than the Himalayas, the Eocene-Oligocene sandstones of the South Sistan Basin in Iran exhibit detrital zircon U-Pb ages similar to those in West Makran but the ε-$Hf_{(t)}$ values of Late Cretaceous zircons are more positive than the ε-$Hf_{(t)}$ values of West Makran contemporaneous zircons (figs. 10, 11 and table). Zircon U-Pb ages of the Zahedan-Shah Kuh granitic belt in SE Iran (Mohammadi and others, 2016a) and Oman ophiolites (Chen and Pallister, 1981; Tilton and others, 1981; Warren and others, 2005; Rioux and others, 2012) differ from West Makran detrital zircons (table 1). Misfits of zircon U-Pb ages and Hf isotopic composition exclude all of these areas as sources of Late Cretaceous-Miocene detritus of the West Makran Basin.

Generally the detrital zircon shapes, ages and ε-$Hf_{(t)}$ values of West Makran Eocene-Miocene sandstones are consistent with what is known in eastern Iranian Makran (figs. 8, 9, 10, 11 and table 1; Mohammadi and others, 2016c). We therefore argue that the source of these sediments was a magmatic arc to the north of the Makran Basin during the Cretaceous-Eocene times. These observations fit tectonic reconstructions dating the beginning of the Makran subduction in the Late Cretaceous (Berberian and Berberian, 1981; McCall, 1997; Mohammadi, ms, 2015), giving rise to the Makran Accretionary Wedge and to a magmatic arc further north.

The configuration of Tethys in the Mesozoic and Early Cenozoic involves a continental sliver extending from the Sanandaj-Sirjan/Bajgan-Durkan Complexes (SSBDC, fig. 1). This continental sliver stretched between two oceanic basins, the inner (North Makran) ocean to the north and the outer (Neo-Tethys) ocean to the south (Şengör and others, 1988; McCall, 1995). Remnants of Neo-Tethys are today's Gulf of Oman and Arabian Sea. The northern, inner oceanic basin is represented by the North Makran ophiolites (Hunziker and others, 2015). The Mid-Jurassic detrital zircons linked to rifting magmas support opening of the inner oceanic basin at that time. This oceanic basin began subducting below the Central Iranian Block in the Early Cretaceous and closed in the Paleogene (Hunziker, 2014). Late Cretaceous-Eocene detrital zircons dated in this work are attributed to the related North Makran Magmatic Arc who may have been entirely subducted or buried beneath the UDMA and Jaz Murian Basin (fig. 1).

CONCLUSION

The present work assessed the provenance of detrital material of the West Makran accretionary wedge including Late Cretaceous to Miocene turbiditic and deltaic-shelf sandstones. Over 2300 detrital zircons yield a spectrum of U-Pb ages of protolith from Archean to Miocene (3.3 Ga–18 Ma) with main peaks in Middle Jurassic (165 Ma), Early to Late Cretaceous (105 Ma, 95 Ma, 89 Ma, 75 Ma and 66 Ma), Eocene (48 Ma) and a minor peak in Miocene (22 Ma). The Middle Jurassic ε-$Hf_{(t)}$ values range from -1.9 to -8.2. The Late Cretaceous-Eocene ε-$Hf_{(t)}$ values range between -11.5 and $+16.3$. The combined Hf isotope data and U-Pb ages indicate that protolith rocks belonged to a Middle Jurassic rift (opening of North Makran, inner ocean) and a Late Cretaceous-Eocene continental magmatic arc (subducting of the inner ocean below Central Iran). Sources within the Central Iran blocks delivered older zircons. Heavy mineral assemblages and Cr-spinel imply ophiolites as subsidiary sediment source. These ophiolites developed in the rift system to the north of the study area. These results do not support the hypothesis that West Makran detritus was supplied from Himalayan sources in a paleo-Indus submarine fan delta complex. Instead, like in the

eastern Iranian Makran, Eocene-Oligocene detritus was transported southward into the Makran Basin from a nearby complex of rift related magmatic rocks, continental arc and ophiolites. Miocene detritus were recycled from accreted Eocene-Oligocene sandstones with a possible addition from the Urmia-Dokhtar Magmatic Arc.

ACKNOWLEDGMENTS

This study was funded by the Forschungsreserven/J.-P. Burg (grant no. 2-78159-99) and the Swiss National Fond (grant no. 2-77644-09). The authors are indebted to Dr. Abdollah Saidi and the National Iranian Oil Company (NIOC) for efficient support during fieldwork. We gratefully acknowledge Vincenzo Picotti and Jonas Ruh for their help in the field, and Miriam Cobianchi for fossil determination. Thanks are due to Jakub Sliwinski for his support on the Laser ablation ICP-MS, Karsten Kunze for his assistance for CL and BSC imaging, and Remy Lüchinger for his help on sandstone thin sections.

APPENDIX I

Sandstone Thin Section

Modal framework grain analysis of sandstones was performed by applying the Gazzi-Dickinson method on thin sections stained for feldspars and carbonates (Dickson, 1966; Norman, 1974). More than 300 detrital grains were counted in each thin section for statistical reliability (Folk, 1980). The Zuffa method has been used to count lithic fragments (Zuffa, 1985). Minerals larger than 0.063 mm within rock fragments were counted as monomineralic grains. Results were converted to percentages for compositional comparison (table SI2; Weltje and von Eynatten, 2004). Data are displayed in five standard complementary triangular diagrams (QFL, QmFLt, LvhLsLm, QmPK and QpLvLsm; Dickinson, 1985; Folk, 1980).

Heavy Mineral Separation

Approximately 2 to 3 kg of fresh rock was collected of each sample for heavy mineral analysis. To obtain transparent heavy mineral fractions (density $\geq$ 2.9 g/cm3 and typically $<$ 1% of bulk rock), sandstones were crushed with the SelFrag apparatus batch equipment using high voltage (130–150 kV) pulse power technology, which liberates morphologically intact minerals. From the $<$ 2 mm sieved fraction, carbonate was dissolved in warm (60–70 °C) 10% acetic acid. Heavy minerals were pulled out in separation funnels (Mange and Maurer, 1992) from 0.063 mm to 0.4 mm sieve fractions using bromoform (density 2.88 g/cm^3). The bulk heavy mineral fractions were mounted in piperine (Martens, 1932) between a glass slab and a cover. Identification and quantification were carried out under a petrographic microscope by applying the mid-point ribbon and fleet counting methods. At least 200 grains were counted per sample (Mange and Maurer, 1992; table S3, http://earth.geology.yale.edu/%7eajs/SupplementaryData/2017/Mohammadi/TableS3.xlsx).

Detrital Zircon Separation and Dating

Detrital zircons were extracted from approximately 2 to 3 kg of SelFrag-crushed sandstone, using standard mineral separation techniques such as, dissolution of carbonate cement in cold hydrochloric acid, and heavy liquid separation (methylene iodide, density 3.32 g/cm^3). Handpicked zircons of three different sizes (fine, medium and coarse) were mounted in epoxy blocks and polished down to core exposition. All analyzed zircons were controlled and photographed with cathodoluminescence (CL) and backscattered-electron imaging (Jackson and others, 2004) to determine internal structures and inclusions of grains prior to isotopic analysis. The CL and BSE images were taken from a split screen on a CamScan CS44 scanning electron microscope at ETH in Zurich.

The Laser ablation ICP-MS analyses were performed on an Elan 6100 DRC instrument coupled to an in-house built 193 nm Excimer laser at the ETH Zurich. Helium gas (1.1 l/min) is used as carrier gas in the ablation cell. The laser was run at a pulse rate of 10 Hz with an energy of 0.5 mJ/pulse and a spot size of 30 μm. The accuracy and reproducibility of each analytical run were monitored by periodic measurements of the standard GJ-1, with $^{207}Pb/^{206}Pb$ age of 608.5 $\pm$ 0.4 Ma (Jackson and others, 2004). Data reduction was performed using the GLITTER software to calculate the relevant isotopic ratios, ages and errors (Van Achterbergh and others, 2001). Concordia and frequency probability diagrams were performed using ISOPLOT v.3.0 (Ludwig, 2003). A Concordant age is given by the overlapping of the error ellipse with the Concordia age curve. In this study, only concordant ages are considered. The frequency U-Pb age

distribution diagram or probability density plot described by (Ludwig, 2003) includes a histogram representing the number of individual zircon grains within a short age range and the probability curve depicts the mean age peaks of the age populations in one sample (table S4, http://earth.geology.yale.edu/%7eajs/SupplementaryData/2017/Mohammadi/TableS4.xlsx).

In-Situ Hafnium Isotope Ratios

In-situ Hf isotope analysis was performed on a Nu plasma MC-ICP-MS (Nu instrument Ltd) attached to a 193 nm UV ArF Excimer laser, at ETH Zurich on the same zircon grains used for U-Pb dating. Ablation was carried using He as a sweep gas with a flow rate of 0.8–1.11 l/min and combined with Ar (~0.7 l/min) using a 40 μm spot size and a 5 Hz laser pulse repetition rate. The energy density used was 10–20 J cm^{22} and each ablation was preceded by a 40 second background measurement, and ablated zircon was measured within 60 s. Lutetium and Yb were analyzed in order to correct for isobaric interferences on ^{176}Hf using $^{173}Yb/^{176}Yb = 0.79618$ and $^{175}Lu/^{176}Lu = 0.026549$ (Chu and others, 2002). The βHf and βYb mass bias coefficients were calculated using an exponential law from measured $^{179}Hf/^{177}Hf$ and $^{173}Yb/^{171}Yb$ respectively and using natural abundance reference values ($^{179}Hf/^{177}Hf = 0.7325$; $^{173}Yb/^{171}Yb = 1.132685$; (Chu and others, 2002). The Lu mass bias fractionation was assumed to be the same as Yb. The accuracy and precision of the data obtained was monitored through the systematic measurements of the well characterized Temora-2 (0.282686; Woodhead and Hergt, 2005), Mud Tank (0.282507; Woodhead and Hergt, 2005) and Plešovice (0.282482; Sláma and others, 2008) reference natural zircon samples with known Hf isotopic compositions. The standard reference materials were chosen in order to have a range in Yb/Hf ratios to test the accuracy of the ^{176}Yb correction following the protocols of Fisher and others (2014). Repeated standard analysis yielded results for the analytical session: Temora-2 = 0.282683, n = 37; Plešovice = 0.282474, n = 17; Mud Tank = 0.282494, n = 21, which are good agreement with the published (table SI5; Blichert-Toft and Albarède, 1997).

The supplementary data tables:

http://earth.geology.yale.edu/%7eajs/SupplementaryData/2017/Mohammadi/TableS1.xlsx
http://earth.geology.yale.edu/%7eajs/SupplementaryData/2017/Mohammadi/TableS2.xlsx
http://earth.geology.yale.edu/%7eajs/SupplementaryData/2017/Mohammadi/TableS3.xlsx
http://earth.geology.yale.edu/%7eajs/SupplementaryData/2017/Mohammadi/TableS4.xlsx
http://earth.geology.yale.edu/%7eajs/SupplementaryData/2017/Mohammadi/TableS5.xlsx

REFERENCES

Berberian, F., and Berberian, M., 1981, Tectono-plutonic episodes in Iran, Zagros, Hindu Kush, Himalaya: Geodynamic Evolution, Volume 3: Washington, DC, AGU, p. 5–32.

Blichert-Toft, J., and Albarède, F., 1997, The Lu-Hf isotope geochemistry of chondrites and the evolution of the mantle-crust system: Earth and Planetary Science Letters, v. 148, n. 1–2, p. 243–258, https://doi.org/10.1016/S0012-821X(97)00040-X

Bouilhol, P., Jagoutz, O., Hanchar, J. M., and Dudas, F. O., 2013, Dating the India–Eurasia collision through arc magmatic records: Earth and Planetary Science Letters, v. 366, p. 163–175, https://doi.org/10.1016/j.epsl.2013.01.023

Burg, J.-P., Dolati, A., Bernoulli, D., and Smit, J., 2013, Structural style of the Makran Tertiary accretionary complex in SE-Iran, *in* Al Hosani, K., Roure, F., Ellison, R., and Lokier, S., editors, Lithosphere dynamics and sedimentary basins: The Arabian Plate and Analogues: Heidelberg, Springer Verlag, Frontiers in Earth Science, p. 239–259, https://doi.org/10.1007/978-3-642-30609-9_12

Carter, A., Najman, Y., Bahroudi, A., Bown, P., Garzanti, E., and Lawrence, R. D., 2010, Locating earliest records of orogenesis in western Himalaya: Evidence from Paleogene sediments in the Iranian Makran region and Pakistan Katawaz basin: Geology, v. 38, n. 9, p. 807–810, https://doi.org/10.1130/G31087.1

Chen, J. H., and Pallister, J. S., 1981, Lead isotopic studies of the Samail ophiolite, Oman: Journal of Geophysical Research–Solid Earth, v. 86, n. B4, p. 2699–2708, https://doi.org/10.1029/JB086iB04p02699

Chiu, H.-Y., Chung, S.-L., Zarrinkoub, M. H., Mohammadi, S. S., Khatib, M. M., and Iizuka, Y., 2013, Zircon U–Pb age constraints from Iran on the magmatic evolution related to Neotethyan subduction and Zagros orogeny: Lithos, v. 162–163, p. 70–87, https://doi.org/10.1016/j.lithos.2013.01.006

Chu, M.-F., Chung, S.-L., Song, B., Liu, D., O'Reilly, S. Y., Pearson, N. J., Ji, J., and Wen, D.-J., 2006, Zircon U-Pb and Hf isotope constraints on the Mesozoic tectonics and crustal evolution of southern Tibet: Geology, v. 34, n. 9, p. 745–748, https://doi.org/10.1130/G22725.1

Chu, N.-C., Taylor, R. N., Chavagnac, V., Nesbitt, R. W., Boella, R. M., Milton, J. A., German, C. R., Bayon, G., and Burton, K., 2002, Hf isotope ratio analysis using multi-collector inductively coupled plasma mass spectrometry: An evaluation of isobaric interference corrections: Journal of Analytical Atomic Spectrometry, v. 17, n. 12, p. 1567–1574, https://doi.org/10.1039/b206707b

Coleman, R. G., DeBari, S., and Peterman, Z., 1992, A-type granite and the Red Sea opening: Tectonophysics, v. 204, n. 1–2, p. 27–40, https://doi.org/10.1016/0040-1951(92)90267-A

Critelli, S., De Rosa, R., and Platt, J. P., 1990, Sandstone detrital modes in the Makran accretionary wedge,

southwest Pakistan: Implications for tectonic setting and long-distance turbidite transportation: Sedimentary Geology, v. 68, n. 4, p. 241–260, https://doi.org/10.1016/0037-0738(90)90013-J
DeCelles, P., Gehrels, G. E., Quade, J., LaReau, B., and Spurlin, M., 2000, Tectonic implications of U-Pb zircon ages of the Himalayan orogenic belt in Nepal: Science, v. 288, n. 5465, p. 497–499, https://doi.org/10.1126/science.288.5465.497
DeCelles, P. G., Kapp, P., Quade, J., and Gehrels, G. E., 2011, Oligocene–Miocene Kailas basin, southwestern Tibet: Record of postcollisional upper-plate extension in the Indus-Yarlung suture zone: Geological Society of America Bulletin, v. 123, n. 7–8, p. 1337–1362, https://doi.org/10.1130/B30258.1
Deer, W. A., Howie, R. A., and Zussman, J., 1992, An introduction to the rock-forming minerals: London, Longman Scientific and Technical, 696 p.
DeMets, C., Gordon, R. G., and Argus, D. F., 2010, Geologically current plate motions: Geophysical Journal International, v. 181, n. 1, p. 1–80, https://doi.org/10.1111/j.1365-246X.2009.04491.x
Dickinson, W. R., 1985, Interpreting provenance relations from detrital modes of sandstones, Provenance of arenites: The Netherlands, Springer, NATO ASI Series, v. 148, p. 333–361, https://doi.org/10.1007/978-94-017-2809-6_15
Dickinson, W. R., and Suczek, C. A., 1979, Plate tectonics and sandstone compositions: AAPG Bulletin, v. 63, n. 12, p. 2164–2182.
Dickson, J. A. D., 1966, Carbonate identification and genesis as revealed by staining: Journal of Sedimentary Research, v. 36, n. 2, p. 491–505, https://doi.org/10.1306/74D714F6-2B21-11D7-8648000102C1865D
Dolati, A., ms, 2010, Stratigraphy, structural geology and low-temperature thermochronology across the Makran accretionary wedge in Iran: Zurich, Switzerland, ETH Zurich, Ph. D. thesis, 168 p., https://doi.org/10.3929/ethz-a-006226348
Ellouz-Zimmermann, N., Deville, E., Müller, C., Lallemant, S., Subhani, A. B., and Tabreez, A. R., 2007a, Impact of sedimentation on convergent margin tectonics: Example of the Makran Accretionary Prism (Pakistan), *in* Lacombe, O., Lavé, J., Roure, F., and Vergés, J., editors, Thrust Belts and Foreland Basins: From fold kinematics to hydrocarbon systems: Berlin, Springer Verlag, p. 327–350, https://doi.org/10.1007/978-3-540-69426-7_17
Ellouz-Zimmermann, N., Lallemant, S. J., Castilla, R., Mouchot, N., Leturmy, P., Battani, A., Buret, C., Cherel, L., Desaubliaux, G., Deville, E., Ferrand, J., Lügcke, A., Mahieux, G., Mühr, P. Pierson-Wickmann, A. C., Robion, P., Schmitz, J., Danish, M., Hasany, S., Shahzad, A., and Tabreez, A., 2007b, Offshore frontal part of the Makran Accretionary prism: The Chamak survey (Pakistan), Thrust Belts and Foreland Basins: Berlin, Springer, p. 351–366, https://doi.org/10.1007/978-3-540-69426-7_18
Fakhri, M., 1994, Bandar Abbas geological quadrangle map: National Iraninan Oil Company, 1:250,000.
Fisher, C. M., Vervoort, J. D., and Hanchar, J. M., 2014, Guidelines for reporting zircon Hf isotopic data by LA-MC-ICPMS and potential pitfalls in the interpretation of these data: Chemical Geology, v. 363, p. 125–133, https://doi.org/10.1016/j.chemgeo.2013.10.019
Folk, R. L., 1980, Petrology of sedimentary rocks: Austin, Texas, Hemphill Publishing Company, 184 p.
Fraser, J. E., Searle, M. P., Parrish, R. R., and Noble, S. R., 2001, Chronology of deformation, metamorphism, and magmatism in the southern Karakoram Mountains: Geological Society of America Bulletin, v. 113, n. 11, p. 1443–1455, https://doi.org/10.1130/0016-7606(2001)113<1443:CODMAM>2.0.CO;2
Gehrels, G., Kapp, P., DeCelles, P., Pullen, A., Blakey, R., Weislogel, A., Ding, L., Guynn, J., Martin, A., McQuarrie, N., and Yin, Y., 2011, Detrital zircon geochronology of pre–Tertiary strata in the Tibetan–Himalayan orogen: Tectonics, v. 30, n. 5, https://doi.org/10.1029/2011TC002868
Gradstein, F. M., Ogg, G., and Schmitz, M., 2012, The Geologic Time Scale 2012, 2-Volume Set: The Netherlands, Elsevier, 1176 p.
Grando, G., and McClay, K., 2007, Morphotectonics domains and structural styles in the Makran accretionary prism, offshore Iran: Sedimentary Geology, v. 196, n. 1–4, p. 157–179, https://doi.org/10.1016/j.sedgeo.2006.05.030
Griffin, W. L., Pearson, N. J., Belousova, E., Jackson, S. E., Van Achterbergh, E., O'Reilly, S. Y., and Shee, S. R., 2000, The Hf isotope composition of cratonic mantle: LAM-MC-ICPMS analysis of zircon megacrysts in kimberlites: Geochimica et Cosmochimica Acta, v. 64, n. 1, p. 133–147, https://doi.org/10.1016/S0016-7037(99)00343-9
Grigsby, J., Kassi, A., and Khan, A., 2004 Petrology and geochemistry of the Oligocene-early Miocene Panjgur Formation and upper Cretaceous-Palaeocene Ispikan Formation and Wakai mélange in the Makran Accretionary Belt, southwest Pakistan: Geological Society of America Abstracts with Programs, v. 36, n. 5, p. 372.
Hassanzadeh, J., Stockli, D. F., Horton, B. K., Axen, G. J., Stockli, L. D., Grove, M., Schmitt, A. K., and Walker, J. D., 2008, U-Pb zircon geochronology of late Neoproterozoic–Early Cambrian granitoids in Iran: Implications for paleogeography, magmatism, and exhumation history of Iranian basement: Tectonophysics, v. 451, n. 1–4, p. 71–96, https://doi.org/10.1016/j.tecto.2007.11.062
Henderson, A. L., Najman, Y., Parrish, R., BouDagher□Fadel, M., Barford, D., Garzanti, E., and Andò, S., 2010, Geology of the Cenozoic Indus Basin sedimentary rocks: Paleoenvironmental interpretation of sedimentation from the western Himalaya during the early phases of India–Eurasia collision: Tectonics, v. 29, n. 6, https://doi.org/10.1029/2009TC002651
Heuberger, S., Schaltegger, U., Burg, J.-P., Villa, I. M., Frank, M., Dawood, H., Hussain, S., and Zanchi, A., 2007, Age and isotopic constraints on magmatism along the Karakoram-Kohistan Suture Zone, NW Pakistan: Evidence for subduction and continued convergence after India-Asia collision: Swiss Journal of Geosciences, v. 100, n. 1, p. 85–107, https://doi.org/10.1007/s00015-007-1203-7
Honegger, K., Dietrich, V., Frank, W., Gansser, A., Thöni, M., and Trommsdorff, V., 1982, Magmatism and metamorphism in the Ladakh Himalayas (the Indus-Tsangpo suture zone): Earth and Planetary Science Letters, v. 60, n. 2, p. 253–292, https://doi.org/10.1016/0012-821X(82)90007-3
Horton, B. K., Hassanzadeh, J., Stockli, D. F., Axen, G. J., Gillis, R. J., Guest, B., Amini, A., Fakhari, M. D.,

Zamanzadeh, S. M., and Grove, M., 2008, Detrital zircon provenance of Neoproterozoic to Cenozoic deposits in Iran: Implications for chronostratigraphy and collisional tectonics: Tectonophysics, v. 451, n. 1–4, p. 97–122, https://doi.org/10.1016/j.tecto.2007.11.063

Hunziker, D., ms, 2014, Magmatic and metamorphic history of the North Makran Ophiolites and Blueschists (SE Iran): Influence of Fe3+/Fe2+ ratios in blueschist facies minerals on geothermobarometric calculations: Zurich, Switzerland, Ph. D. thesis, ETH Zürich, Nr. 21778, https://doi.org/10.3929/ethz-a-010336252

Hunziker, D., Burg, J. P., Bouilhol, P., and von Quadt, A., 2015, Jurassic rifting at the Eurasian Tethys margin: Geochemical and geochronological constraints from granitoids of North Makran, southeastern Iran: Tectonics, v. 34, n. 3, p. 571–593, https://doi.org/10.1002/2014TC003768

Jackson, S. E., Pearson, N. J., Griffin, W. L., and Belousova, E. A., 2004, The application of laser ablation-inductively coupled plasma-mass spectrometry to *in situ* U–Pb zircon geochronology: Chemical Geology, v. 211, n. 1–2, p. 47–69, https://doi.org/10.1016/j.chemgeo.2004.06.017

Jain, A. K., and Singh, S., 2008, Tectonics of the southern Asian Plate margin along the Karakoram Shear Zone: Constraints from field observations and U–Pb SHRIMP ages: Tectonophysics, v. 451, n. 1–4, p. 186–205, https://doi.org/10.1016/j.tecto.2007.11.048

Ji, W.-Q., Wu, F.-Y., Chung, S.-L., Li, J.-X., and Liu, C.-Z., 2009, Zircon U–Pb geochronology and Hf isotopic constraints on petrogenesis of the Gangdese batholith, southern Tibet: Chemical Geology, v. 262, n. 3–4, p. 229–245, https://doi.org/10.1016/j.chemgeo.2009.01.020

Kassi, A. M., Khan, A. S., Kelling, G., and Kasi, A. K., 2011, Facies and cyclicity within the Oligocene-Early Miocene Panjgur Formation, Khojak–Panjgur Submarine Fan Complex, south-west Makran, Pakistan: Journal of Asian Earth Sciences, v. 41, n. 6, p. 537–550, https://doi.org/10.1016/j.jseaes.2011.03.007

Kassi, A. M., Kasi, A. K., McManus, J., and Khan, A. S., 2013, Lithostratigraphy, petrology and sedimentary facies of the Late Cretaceous-Palaeocene Ispikan Group, southwestern Makran, Pakistan: Journal of Himalayan Earth Sciences, v. 46, n. 2, p. 49–63.

Kassi, A. M., Grigsby, J. D., Khan, A. S., and Kasi, A. K., 2015, Sandstone petrology and geochemistry of the Oligocene–Early Miocene Panjgur Formation, Makran accretionary wedge, southwest Pakistan: Implications for provenance, weathering and tectonic setting: Journal of Asian Earth Sciences, v. 105, p. 192–207, https://doi.org/10.1016/j.jseaes.2015.03.021

Krol, M. A., Zeitler, P. K., and Copeland, P., 1996, Episodic unroofing of the Kohistan Batholith, Pakistan: Implications from K–feldspar thermochronology: Journal of Geophysical Research: Solid Earth (1978–2012), v. 101, n. B12, p. 28149–28164, https://doi.org/10.1029/96JB01503

Ludwig, K. R., 2003, User's manual for Isoplot 3.00: : geochronological toolkit for Microsoft Excel: Berkeley, California, Berkeley Geochronology Center Special Publication, v. 4., 74 p.

Mange, M. A., and Maurer, H. F., 1992, Heavy minerals in colour: London, England, Chapman & Hall, 147 p., https://doi.org/10.1007/978-94-011-2308-2

Martens, J. H. C., 1932, Piperine as an immersion medium in sedimentary petrography: American Mineralogist, v. 17, n. 5, p. 198–199.

Masson, F., Anvari, M., Djamour, Y., Walpersdorf, A., Tavakoli, F., Daignières, M., Nankali, H., and Van Gorp, S., 2007, Large-scale velocity field and strain tensor in Iran inferred from GPS measurements: New insight for the present-day deformation pattern within NE Iran: Geophysical Journal International, v. 170, n. 1, p. 436–440, https://doi.org/10.1111/j.1365-246X.2007.03477.x

McCall, G. J. H., 1983, Mélanges of the Makran, southeastern Iran, *in* McCall, G. J. H., editor, Ophiolitic and related mélanges: Benchmark Papers in Geology, v. 66, p. 292–299.

——— 1985a, Explanatory text of the Fannuj quadrangle map 1:250,000, Tehran: Geological Survey of Iran, 416 p.

——— 1985b, Area report - East Iran Project-Area No: 1 (North Makran & South Baluchestan): Tehran, Heidary, 636 p.

——— 1985c, Explanatory text of the Tahruie quadrangle map 1:250,000: Tehran, Geological Survey of Iran, Heidary, 454 p.

——— 1985d, Explanatory text of the Minab quadrangle map 1:250,000: Tehran, Geological Survey of Iran, Heidary.

——— 1995, The inner Mesozoic to Eocene ocean of South and Central Iran and the associated microcontinents: GEOTECTONICS C/C OF GEOTEKTONIKA, v. 29, p. 490–497.

——— 1997, The geotectonic history of the Makran and adjacent areas of southern Iran: Journal of Asian Earth Sciences, v. 15, n. 6, p. 517–531, https://doi.org/10.1016/S0743-9547(97)00032-9

McCall, G., and Kidd, R., 1982, The Makran, Southeastern Iran: The anatomy of a convergent plate margin active from Cretaceous to Present: Geological Society, London, Special Publications, v. 10, n. 1, p. 387–397, https://doi.org/10.1144/GSL.SP.1982.010.01.26

Mohammadi, A., ms, 2015, Provenance analysis and detrital zircons: Keys to the tectonic setting of the Makran and Sistan basins in Iran: Zürich, Switzerland, ETH Zürich, Ph. D. thesis, 124 p.

Mohammadi, A., Burg, J.-P., Bouilhol, P., and Ruh, J., 2016a, U–Pb geochronology and geochemistry of Zahedan and Shah Kuh plutons, southeast Iran: Implication for closure of the South Sistan suture zone: Lithos, v. 248–251, p. 293–308, https://doi.org/10.1016/j.lithos.2016.02.003

Mohammadi, A., Burg, J.-P., and Winkler, W., 2016b, Detrital zircon and provenance analysis of Eocene–Oligocene strata in the South Sistan suture zone, southeast Iran: Implications for the tectonic setting: Lithosphere, v. 8, n. 6, p. 615–632, https://doi.org/10.1130/L538.1

Mohammadi, A., Burg, J.-P., Winkler, W., Ruh, J., and von Quadt, A., 2016c, Detrital zircon and provenance analysis of Late Cretaceous− Miocene onshore Iranian Makran strata: Implications for the tectonic setting: Geological Society of America Bulletin, v. 128, n. 9–10, p. 1481–1499, https://doi.org/10.1130/B31361.1

Nadimi, A., 2007, Evolution of the Central Iranian basement: Gondwana Research, v. 12, n. 3, p. 324–333, https://doi.org/10.1016/j.gr.2006.10.012

Naing, T. T., Bussien, D. A., Winkler, W. H., Nold, M., and Von Quadt, A., 2014, Provenance study on Eocene–Miocene sandstones of the Rakhine Coastal Belt, Indo-Burman Ranges of Myanmar: Geodynamic implications: Geological Society, London, Special Publications, v. 386, n. 1, p. 195–216, https://doi.org/10.1144/SP386.10

Norman, M. B., 1974, Improved techniques for selective staining of feldspar and other minerals using amaranth: US Geological Survey Journal of Research, v. 2, n. 1, p. 73–79.

Parrish, R. R., and Tirrul, R., 1989, U-Pb age of the Baltoro granite, northwest Himalaya, and implications for monazite U-Pb systematics: Geology, v. 17, n. 12, p. 1076–1079, https://doi.org/10.1130/0091-7613(1989)017<1076:UPAOTB>2.3.CO;2

Patchett, P. J., 1983, Importance of the Lu-Hf isotopic system in studies of planetary chronology and chemical evolution: Geochimica et Cosmochimica Acta, v. 47, n. 1, p. 81–91, https://doi.org/10.1016/0016-7037(83)90092-3

Phillips, R. J., Parrish, R. R., and Searle, M. P., 2004, Age constraints on ductile deformation and long-term slip rates along the Karakoram fault zone, Ladakh: Earth and Planetary Science Letters, v. 226, n. 3–4, p. 305–319, https://doi.org/10.1016/j.epsl.2004.07.037

Platt, J. P., Leggett, J. K., Young, J., Raza, H., and Alam, S., 1985, Large-scale sediment underplating in the Makran accretionary prism, southwest Pakistan: Geology, v. 13, n. 7, p. 507–511, https://doi.org/10.1130/0091-7613(1985)13<507:LSUITM>2.0.CO;2

Qayyum, M., Niem, A. R., and Lawrence, R. D., 1996, Newly discovered Paleogene deltaic sequence in Katawaz basin, Pakistan, and its tectonic implications: Geology, v. 24, n. 9, p. 835–838, https://doi.org/10.1130/0091-7613(1996)024<0835:NDPDSI>2.3.CO;2

Qayyum, M., Lawrence, R. D., and Niem, A. R., 1997a, Discovery of the palaeo-Indus delta-fan complex: Journal of the Geological Society, v. 154, n. 5, p. 753–756, https://doi.org/10.1144/gsjgs.154.5.0753

——— 1997b, Molasse-Delta-flysch continuum of the Himalayan orogeny and closure of the Paleogene Katawaz Remnant Ocean, Pakistan: International Geology Review, v. 39, n. 10, p. 861–875, https://doi.org/10.1080/00206819709465306

Qayyum, M., Niem, A. R., and Lawrence, R. D., 2001, Detrital modes and provenance of the Paleogene Khojak Formation in Pakistan: Implications for early Himalayan orogeny and unroofing: Geological Society of America Bulletin, v. 113, n. 3, p. 320–332, https://doi.org/10.1130/0016-7606(2001)113<0320:DMAPOT>2.0.CO;2

Ramezani, J., and Tucker, R. D., 2003, The Saghand region, central Iran: U-Pb geochronology, petrogenesis and implications for Gondwana tectonics: American Journal of Science, v. 303, n. 7, p. 622–665, https://doi.org/10.2475/ajs.303.7.622

Ravikant, V., Wu, F.-Y., and Ji, W.-Q., 2009, Zircon U–Pb and Hf isotopic constraints on petrogenesis of the Cretaceous–Tertiary granites in eastern Karakoram and Ladakh, India: Lithos, v. 110, n. 1–4, p. 153–166, https://doi.org/10.1016/j.lithos.2008.12.013

Rioux, M., Bowring, S., Kelemen, P., Gordon, S., Dudás, F., and Miller, R., 2012, Rapid crustal accretion and magma assimilation in the Oman–UAE ophiolite: High precision U–Pb zircon geochronology of the gabbroic crust: Journal of Geophysical Research-Solid Earth, v. 117, n. B7, https://doi.org/10.1029/2012JB009273

Roddaz, M., Said, A., Guillot, S., Antoine, P.-O., Montel, J.-M., Martin, F., and Darrozes, J., 2011, Provenance of Cenozoic sedimentary rocks from the Sulaiman fold and thrust belt, Pakistan: Implications for the palaeogeography of the Indus drainage system: Journal of the Geological Society, v. 168, n. 2, p. 499–516, https://doi.org/10.1144/0016-76492010-100

Samadian, M. R., and Khan Nazer, N. H., 1999, Jask-Gattan geological quadrangle map: Geological Survey of Iran, scale 1:100,000.

Samadian, M. R., Gharaie, M. H. M., and Karimi Nia, M., 1999, Gabric geological quadrangle map: Geological Survey of Iran, scale 1:100,000.

Samimi Namin, M., McCall, G. J. H., and Huber, H., 1983, Minab geological quadrangle map: Geological Survey of Iran, scale 1:250,000.

Samimi Namin, M., McCall, G. J. H., Huber, H., and Mohajer, G. A., 1982, Taherui geological quadrangle map: Geological Survey of Iran, scale 1:250,000.

Schaltegger, U., Zeilinger, G., Frank, M., and Burg, J. P., 2002, Multiple mantle sources during island arc magmatism: U–Pb and Hf isotopic evidence from the Kohistan arc complex, Pakistan: Terra Nova, v. 14, n. 6, p. 461–468, https://doi.org/10.1046/j.1365-3121.2002.00432.x

Schaltegger, U., Frank, M., and Burg, J.-P., 2003, A 120 million years record of magmatism and crustal melting in the Kohistan Batholith, *in* Proceedings EGS-AGU-EUG Joint Assembly 2003: Abstracts from the meeting held in Nice, France, 6–11 April, 2003, # 6816.

Schärer, U., Hamet, J., and Allègre, C. J., 1984, The Transhimalaya (Gangdese) plutonism in the Ladakh region: A U–Pb and Rb–Sr study: Earth and Planetary Science Letters, v. 67, n. 3, p. 327–339, https://doi.org/10.1016/0012-821X(84)90172-9

Şengör, A. M. C., Altiner, D., Cin, A., Ustaömer, T., and Hsü, K. J., 1988, Origin and assembly of the Tethyside orogenic collage at the expense of Gondwana Land: Geological Society, London, Special Publications, v. 37, n. 1, p. 119–181, https://doi.org/10.1144/GSL.SP.1988.037.01.09

Singh, S., Kumar, R., Barley, M. E., and Jain, A. K., 2007, SHRIMP U–Pb ages and depth of emplacement of Ladakh Batholith, Eastern Ladakh, India: Journal of Asian Earth Sciences, v. 30, n. 3–4, p. 490–503, https://doi.org/10.1016/j.jseaes.2006.12.003

Sláma, J., Košler, J., Condon, D. J., Crowley, J. L., Gerdes, A., Hanchar, J. M., Horstwood, M. S., Morris, G. A., Nasdala, L., Norberg, N., Schaltegger, U., Schoene, B., Turbrett, M. N., and Whitehouse, M. J., 2008,

Plešovice zircon—a new natural reference material for U–Pb and Hf isotopic microanalysis: Chemical Geology, v. 249, n. 1, p. 1–35, https://doi.org/10.1016/j.chemgeo.2007.11.005
Tilton, G. R., Hopson, C. A., and Wright, J. E., 1981, Uranium–lead isotopic ages of the Samail Ophiolite, Oman, with applications to Tethyan ocean ridge tectonics: Journal of Geophysical Research: Solid Earth, v. 86, n. B4, p. 2763–2775, https://doi.org/10.1029/JB086iB04p02763
Upadhyay, R., Frisch, W., and Siebel, W., 2008, Tectonic implications of new U–Pb zircon ages of the Ladakh batholith, Indus suture zone, northwest Himalaya, India: Terra Nova, v. 20, n. 4, p. 309–317, https://doi.org/10.1111/j.1365-3121.2008.00822.x
Van Achterbergh, E., Ryan, C., Jackson, S., and Griffin, W., 2001, Data reduction software for LA-ICP-MS, *in* Sylvester, P., editor, Laser-Ablation-ICPMS in the earth sciences—principles and applications: Mineralogical Association of Canada Short Course series, v. 29, p. 239–243.
Vervoort, J. D., and Blichert-Toft, J., 1999, Evolution of the depleted mantle: Hf isotope evidence from juvenile rocks through time: Geochimica et Cosmochimica Acta, v. 63, n. 3–4, p. 533–556, https://doi.org/10.1016/S0016-7037(98)00274-9
Vigny, C., Huchon, P., Ruegg, J.-C., Khanbari, K., and Asfaw, L. M., 2006, Confirmation of Arabia plate slow motion by new GPS data in Yemen: Journal of Geophysical Research-Solid Earth, v. 111, n. B02402, p. https://doi.org/10.1029/2004jb003229
Von Rad, U., Berner, U., Delisle, G., Doose-Rolinski, H., Fechner, N., Linke, P., Lückge, A., Roeser, H. A., Schmaljohann, R., and Wiedicke, M., 2000, Gas and fluid venting at the Makran accretionary wedge off Pakistan: Geo-Marine Letters, v. 20, n. 1, p. 10–19, https://doi.org/10.1007/s003670000033
Warren, C. J., Parrish, R. R., Waters, D. J., and Searle, M. P., 2005, Dating the geologic history of Oman's Semail ophiolite: Insights from U-Pb geochronology: Contributions to Mineralogy and Petrology, v. 150, n. 4, p. 403–422, https://doi.org/10.1007/s00410-005-0028-5
Weinberg, R. F., and Dunlap, W. J., 2000, Growth and deformation of the Ladakh Batholith, northwest Himalayas: Implications for timing of continental collision and origin of calc□alkaline batholiths: The Journal of Geology, v. 108, n. 3, p. 303–320, https://doi.org/10.1086/314405
Weinberg, R. F., Dunlap, W. J., and Whitehouse, M., 2000, New field, structural and geochronological data from the Shyok and Nubra valleys, northern Ladakh: Linking Kohistan to Tibet: Geological Society, London, Special Publications, v. 170, n. 1, p. 253–275, https://doi.org/10.1144/GSL.SP.2000.170.01.14
Weltje, G. J., and von Eynatten, H., 2004, Quantitative provenance analysis of sediments: Review and outlook: Sedimentary Geology, v. 171, n. 1–4, p. 1–11, https://doi.org/10.1016/j.sedgeo.2004.05.007
Wen, D.-R., Liu, D., Chung, S.-L., Chu, M.-F., Ji, J., Zhang, Q., Song, B., Lee, T.-Y., Yeh, M.-W., and Lo, C.-H., 2008, Zircon SHRIMP U–Pb ages of the Gangdese Batholith and implications for Neotethyan subduction in southern Tibet: Chemical Geology, v. 252, n. 3–4, p. 191–201, https://doi.org/10.1016/j.chemgeo.2008.03.003
White, R. S., 1982, Deformation of the Makran accretionary sediment prism in the Gulf of Oman (north-west Indian Ocean): Geological Society, London, Special Publications, v. 10, n. 1, p. 357–372, https://doi.org/10.1144/GSL.SP.1982.010.01.24
White, R. S., and Klitgord, K., 1976, Sediment deformation and plate tectonics in the Gulf of Oman: Earth and Planetary Science Letters, v. 32, n. 2, p. 199–209, https://doi.org/10.1016/0012-821X(76)90059-5
Woodhead, J. D., and Hergt, J. M., 2005, A preliminary appraisal of seven natural zircon reference materials for *in situ* Hf isotope determination: Geostandards and Geoanalytical Research, v. 29, n. 2, p. 183–195, https://doi.org/10.1111/j.1751-908X.2005.tb00891.x
Wu, F. Y., Clift, P. D., and Yang, J. H., 2007, Zircon Hf isotopic constraints on the sources of the Indus Molasse, Ladakh Himalaya, India: Tectonics, v. 26, n. 2, https://doi.org/10.1029/2006TC002051
Yuan, H.-L., Gao, S., Dai, M.-N., Zong, C.-L., Günther, D., Fontaine, G. H., Liu, X.-M., and Diwu, C. R., 2008, Simultaneous determinations of U–Pb age, Hf isotopes and trace element compositions of zircon by excimer laser-ablation quadrupole and multiple-collector ICP-MS: Chemical Geology, v. 247, n. 1–2, p. 100–118, https://doi.org/10.1016/j.chemgeo.2007.10.003
Zhu, D.-C., Pan, G.-T., Chung, S.-L., Liao, Z.-L., Wang, L.-Q., and Li, G.-M., 2008, SHRIMP zircon age and geochemical constraints on the origin of Lower Jurassic volcanic rocks from the Yeba Formation, southern Gangdese, South Tibet: International Geology Review, v. 50, n. 5, p. 442–471, https://doi.org/10.2747/0020-6814.50.5.442
Zhuang, G., Najman, Y., Guillot, S., Roddaz, M., Antoine, P.-O., Métais, G., Carter, A., Marivaux, L., and Solangi, S. H., 2015, Constraints on the collision and the pre-collision tectonic configuration between India and Asia from detrital geochronology, thermochronology, and geochemistry studies in the lower Indus basin, Pakistan: Earth and Planetary Science Letters, v. 432, p. 363–373, https://doi.org/10.1016/j.epsl.2015.10.026
Zuffa, G. G., 1985, Optical analyses of arenites: Influence of methodology on compositional results, *in* Zuffa, G. G., editor, Provenance of arenites: Netherlands, Springer, NATO ASI Series, v. 148, p. 165–189, https://doi.org/10.1007/978-94-017-2809-6_8